

## INNATE IMMUNE SYSTEM

C/EBP $\beta$  regulates lipid metabolism and *Pparg* isoform 2 expression in alveolar macrophages

Dorothea Dörr<sup>1,2</sup>, Benedikt Obermayer<sup>3</sup>, January Mikolaj Weiner<sup>3</sup>, Karin Zimmermann<sup>1</sup>, Chiara Anania<sup>4</sup>, Lisa Katharina Wagner<sup>1</sup>, Ekaterini Maria Lyras<sup>1</sup>, Valeriia Sapozhnikova<sup>1</sup>, David Lara-Astiaso<sup>5</sup>, Felipe Prósper<sup>6,7</sup>, Roland Lang<sup>8</sup>, Darío G. Lupiáñez<sup>4</sup>, Dieter Beule<sup>3</sup>, Uta E. Höpken<sup>1</sup>, Achim Leutz<sup>1,2</sup>, Alexander Mildner<sup>1,9,10\*</sup>

Pulmonary alveolar proteinosis (PAP) is a syndrome characterized by accumulation of surfactant lipoproteins within the lung alveoli. Alveolar macrophages (AMs) are crucial for surfactant clearance, and their differentiation depends on colony-stimulating factor 2 (CSF2), which regulates the establishment of an AM-characteristic gene regulatory network. Here, we report that the transcription factor CCAAT/enhancer binding protein  $\beta$  (C/EBP $\beta$ ) is essential for the development of the AM identity, as demonstrated by transcriptome and chromatin accessibility analysis. Furthermore, C/EBP $\beta$ -deficient AMs showed severe defects in proliferation, phagocytosis, and lipid metabolism, collectively resulting in a PAP-like syndrome. Mechanistically, the long C/EBP $\beta$  protein variants LAP\* and LAP together with CSF2 signaling induced the expression of *Pparg* isoform 2 but not *Pparg* isoform 1, a molecular regulatory mechanism that was also observed in other CSF2-primed macrophages. These results uncover C/EBP $\beta$  as a key regulator of AM cell fate and shed light on the molecular networks controlling lipid metabolism in macrophages.

## INTRODUCTION

Tissue-resident macrophages (TRMs) are immune sentinels and also serve a critical function within tissues to maintain homeostasis. Development and specialization of these cells are adjusted to the physiological needs of their organ of residence. Hence, alveolar macrophages (AMs), the resident macrophages in the lung alveoli, play an essential role in the maintenance of lung homeostasis, including the clearance of surfactant lipoproteins (1). Impaired degradation of surfactant lipoproteins by AMs results in the accumulation of excessive surfactant within the alveolar space and leads to the development of pulmonary alveolar proteinosis (PAP), a syndrome associated with impaired respiratory function and increased susceptibility to pulmonary infections (2).

AMs are locally self-maintaining cells that are established during embryogenesis and remain largely independent of circulating bone marrow (BM)-derived monocyte replenishment under physiological conditions (3). In mice, liver-derived fetal monocytes (F-Mo) start to colonize the lung around day 14 of embryonic development (E14). Once in the pulmonary tissue, F-Mo are exposed to environmental lung factors that direct their differentiation into immature

AMs (pre-AMs), which begin to accumulate around E18 and subsequently give rise to mature AMs during the first postnatal days (4, 5).

Colony-stimulating factor 2 (CSF2; also known as granulocyte-macrophage CSF), which is produced by alveolar type II epithelial cells (6), is an indispensable growth factor involved in the differentiation of F-Mo and pre-AMs into mature AMs. Mice and humans that lack functional CSF2 signaling fail to develop AMs and, as a consequence, establish PAP syndrome (2). It was previously reported that in AMs, CSF2 signaling induces the expression of the transcription factor (TF) peroxisome proliferator-activated receptor  $\gamma$  (PPAR $\gamma$ ), which subsequently directs the establishment of the AM-characteristic transcriptional identity and their tissue-specific function (7). Accordingly, adult *Pparg*-deficient animals only harbor nonclassical AM-like cells that display phenotypical alterations, including defects in lipid metabolism and accumulation of surfactant lipoproteins, and develop a PAP-like phenotype (7).

The TF CCAAT/enhancer binding protein  $\beta$  (C/EBP $\beta$ ) is a regulator of adipocyte differentiation and of myeloid cell-mediated inflammatory processes, such as emergency granulopoiesis (8–10). Moreover, the development of a few myeloid populations, namely, blood-resident Ly6C<sup>-</sup> monocytes and peritoneal macrophages (PMs), has been described to be C/EBP $\beta$  dependent under homeostatic conditions (11, 12). AM cell numbers were also reported to be affected by C/EBP $\beta$  deficiency (12). However, the exact molecular function of C/EBP $\beta$  in AM biology and its potential regulatory interplay with other key AM factors remain unknown.

Here, we unravel the function and molecular mechanisms of C/EBP $\beta$  in AMs. AMs from adult *Cebpb*-deficient mice showed impaired phagocytosis, a dysregulated lipid metabolism, and attenuated proliferation, collectively accumulating in a PAP-like pathology. Similar changes were detected in a transgenic mouse line that expresses only the truncated, short isoform of C/EBP $\beta$ , liver-enriched inhibiting protein (LIP). Furthermore, our data demonstrate that

<sup>1</sup>Max-Delbrück-Center for Molecular Medicine in Helmholtz Association (MDC), Berlin, Germany. <sup>2</sup>Institute of Biology, Humboldt University of Berlin, Berlin, Germany. <sup>3</sup>Core Unit Bioinformatics, Berlin Institute of Health, Charité-Universitätsmedizin Berlin, Berlin, Germany. <sup>4</sup>Max-Delbrück-Center for Molecular Medicine in Helmholtz Association (MDC), Berlin Institute for Medical Systems Biology (BIMSB), Epigenetics and Sex Development Group, Berlin, Germany. <sup>5</sup>Advanced Genomics Laboratory, Program of Hemato-Oncology, Center for Applied Medical Research (CIMA), University of Navarra, Pamplona, Spain. <sup>6</sup>Program of Regenerative Medicine, Program of Hemato-Oncology, Center for Applied Medical Research (CIMA), University of Navarra, Pamplona, Spain. <sup>7</sup>Instituto de Investigación Sanitaria de Navarra (IdiSNA), Pamplona, Spain. <sup>8</sup>Institute of Clinical Microbiology, Immunology, and Hygiene, Universitätsklinikum Erlangen, Friedrich-Alexander-Universität Erlangen-Nürnberg, Erlangen, Germany. <sup>9</sup>Institute of Biomedicine, Medicity University of Turku, Turku, Finland. <sup>10</sup>InFLAMES Research Flagship Center, University of Turku, Turku, Finland.

\*Corresponding author. Email: alexander.mildner@utu.fi

AMs, in contrast to other TRMs, expressed *Pparg* isoform 2 (*Pparg2*), whereas C/EBP $\beta$ -deficient AMs failed to induce specifically this *Pparg* isoform. We identified CSF2 signaling and C/EBP $\beta$  as necessary cofactors for the induction of *Pparg2* not only in AMs but also in other *Cebpb*-expressing macrophages. These findings suggest a conserved regulatory machinery of lipid metabolism across distinct macrophage subsets. Our results further indicate a dichotomic regulation and function of the PPAR $\gamma$ 1 and PPAR $\gamma$ 2 isoforms.

Collectively, our data establish C/EBP $\beta$  as the missing regulatory link between CSF2 signaling and critical *Pparg2* isoform selection. Targeting the CSF2:C/EBP $\beta$ :PPAR $\gamma$  axis appears as a promising strategy to modulate macrophage-dependent lipid turnover not only in PAP but also in other lipid-associated diseases.

## RESULTS

### C/EBP $\beta$ deficiency leads to AM alterations and PAP-like pathology in mice

The TF C/EBP $\beta$  has been proposed to be involved in the regulation of AM development (12). However, the exact molecular functions of C/EBP $\beta$  and the related regulatory mechanisms in AM biology remain unknown. To investigate the role of C/EBP $\beta$  in AMs, we analyzed the bronchoalveolar lavage fluid (BALF) and lung tissue of mice harboring a constitutive *Cebpb* gene deletion. Using flow cytometry, we found that adult *Cebpb* knockout (KO) mice (7 to 16 weeks) showed reduced numbers of classical AMs (CD11b<sup>low</sup> AMs; F4/80<sup>pos</sup> CD11b<sup>lo</sup> Siglec-F<sup>hi</sup> CD11c<sup>hi</sup>; Fig. 1, A and B; gating strategy in fig. S1, A and B). However, the lungs and BALF of KO mice also contained a population of AMs, which expressed the characteristic AM markers F4/80, Siglec-F, and CD11c and displayed increased expression of the surface marker CD11b (CD11b<sup>high</sup> AMs) (Fig. 1, A to C).

Flow cytometry additionally revealed the presence of high amounts of debris in BALF from C/EBP $\beta$ -deficient mice (Fig. 1A). This finding was in line with an increased turbidity of BALF that was macroscopically visible and quantifiable by optical density measurement at a wavelength of 600 nm (Fig. 1D). A specific enzyme-linked immunosorbent assay (ELISA) revealed elevated concentrations of surfactant protein D (SP-D) in BALF of C/EBP $\beta$  KO mice (Fig. 1E), which is indicative of PAP pathology. BALF cytopins in combination with May-Grünwald-Giemsa staining revealed that AMs from C/EBP $\beta$ <sup>-/-</sup> mice included numerous enlarged cells with a foamy cell-like morphology (Fig. 1F).

To investigate whether C/EBP $\beta$  was required for the embryonic and perinatal development of AMs, we analyzed the lungs of C/EBP $\beta$  KO mice at prenatal stage E18 and postnatal day 3 (P3; gating strategy in fig. S1, C to E). Although the lungs of E18 wild-type (WT) and C/EBP $\beta$  KO embryos showed comparable numbers of F-Mo, C/EBP $\beta$  KO pre-AMs were reduced compared with WT littermates (Fig. 1G). At P3, most WT pre-AMs had developed into mature CD11c<sup>hi</sup> Siglec-F<sup>hi</sup> CD11b<sup>lo</sup> AMs. C/EBP $\beta$  KO pups lacked these cells almost entirely, whereas a population of CD11c<sup>int</sup> Siglec-F<sup>int</sup> CD11b<sup>high</sup> cells, reminiscent of pre-AMs (4), was detected (Fig. 1H). Together, these findings show that prenatal AM development is C/EBP $\beta$  dependent and that C/EBP $\beta$  deficiency leads to the development of a PAP-like phenotype in adult mice.

### C/EBP $\beta$ directs AM identity and lipid metabolic processes

To investigate the role of C/EBP $\beta$  in AMs in more detail, we analyzed fluorescence-activated cell sorting (FACS)-isolated lung Ly6C<sup>high</sup> F-Mo and pre-AMs from WT and C/EBP $\beta$  KO E18 embryos and performed bulk RNA sequencing (RNA-seq;  $n = 3$  or 4 per genotype; gating strategy in fig. S1, C and D; data S1). Comparative analysis of E18 F-Mo revealed only 39 significantly differentially expressed genes (DEGs) between both genotypes [adjusted  $P$  value (adj.  $P$ ) < 0.01 and log<sub>2</sub> fold change ( $|\log_2\text{FC}|$ ) > 2; Fig. 2A]. In contrast, pre-AMs from C/EBP $\beta$  KO mice showed 183 down-regulated genes, including *Pparg*, *Lpl*, and *Abcd2*, whereas 332 genes were up-regulated (e.g., *Etv3*, *Cd209a*, and *Clec10a*; Fig. 2B) compared with WT controls. Gene ontology (GO) enrichment analysis revealed that up-regulated genes in C/EBP $\beta$  KO pre-AMs were associated with processes such as antigen presentation, inflammatory response, and T cell activation, whereas down-regulated genes were involved in foam cell differentiation, lipid storage, and neutral lipid metabolic processes (Fig. 2C).

We next isolated AMs by FACS from BALF of adult WT mice and both CD11b<sup>low</sup> and CD11b<sup>high</sup> AMs from C/EBP $\beta$  KO mice and performed transcriptomic analysis. Comparison of the three populations revealed 1308 significant DEGs (adj.  $P$  < 0.01 and  $|\log_2\text{FC}| > 1$  in at least one pairwise comparison; Fig. 2D and data S1). The DEGs could be divided into three clusters. Cluster 1 (264 genes) comprised genes with the lowest expression in CD11b<sup>high</sup> KO AMs. Genes in cluster 2 (330 genes) were commonly down-regulated in C/EBP $\beta$  KO AMs, and cluster 3 (714 genes) contained up-regulated genes in C/EBP $\beta$  KO AMs. Although we detected transcriptomic differences between CD11b<sup>low</sup> and CD11b<sup>high</sup> KO AMs (mainly represented in cluster 1), principal components (PC) and correlation analyses revealed close similarity between both KO populations, whereas they were both clearly different from WT AMs (Fig. 2E). Of note, the absence of *Cebpb* did not result in a compensatory up-regulation of other *Cebp* family members, nor did it negatively affect the surface expression of CSF2RA and CSF2RB (Fig. 2F and fig. S2A). In contrast, the characteristic AM signature according to a previously identified set of AM-specific genes (13) was diminished in C/EBP $\beta$  KO AMs (fig. S2B).

Next, we performed GO enrichment analysis of the identified DEGs. Cluster 1 revealed no biologically noteworthy results, whereas cluster 2 comprised genes linked to lipid metabolism pathways such as lipid catabolic process and fatty acid metabolic process and included *Fabp1*, *Acox1*, *Olr1*, *Srebf2*, *Lsr*, and the key AM and lipid metabolism regulator *Pparg* (Fig. 2, F and G). Although *Cidec* and *Agnt1* were included in cluster 1, both genes were significantly down-regulated in both KO populations. Cluster 3 showed genes involved in antigen presentation including *Cd74* and *H2-Aa* and genes involved in the GO terms innate immune response, negative regulation of cell proliferation, and chemotaxis. Furthermore, genes required for lipid transport, such as *Abcb1a* and *Trem2*, were increased in KO AMs (Fig. 2, F and G).

Differences in housing conditions, as well as sex-related gene changes, can affect the functions and transcriptomes of macrophages (14, 15). To control for these secondary factors that might influence the phenotype of C/EBP $\beta$  KO AMs, we performed RNA-seq experiments with mice housed in different facilities and with female and male C/EBP $\beta$  KO mice with their respective controls (fig. S2, C to F). Housing- and sex-specific differences were detectable in C/EBP $\beta$ -deficient AMs, yet core transcriptomic changes,

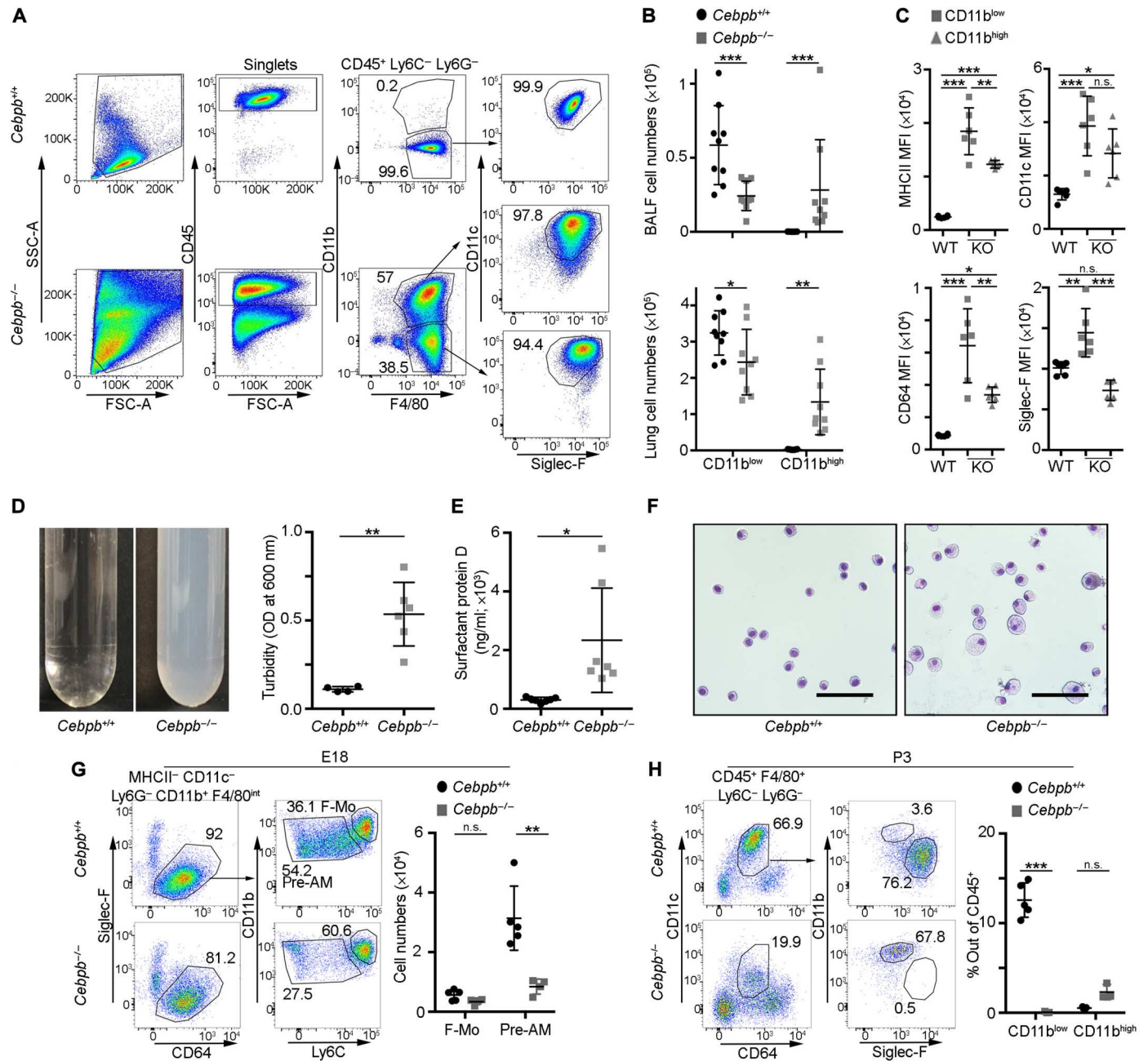
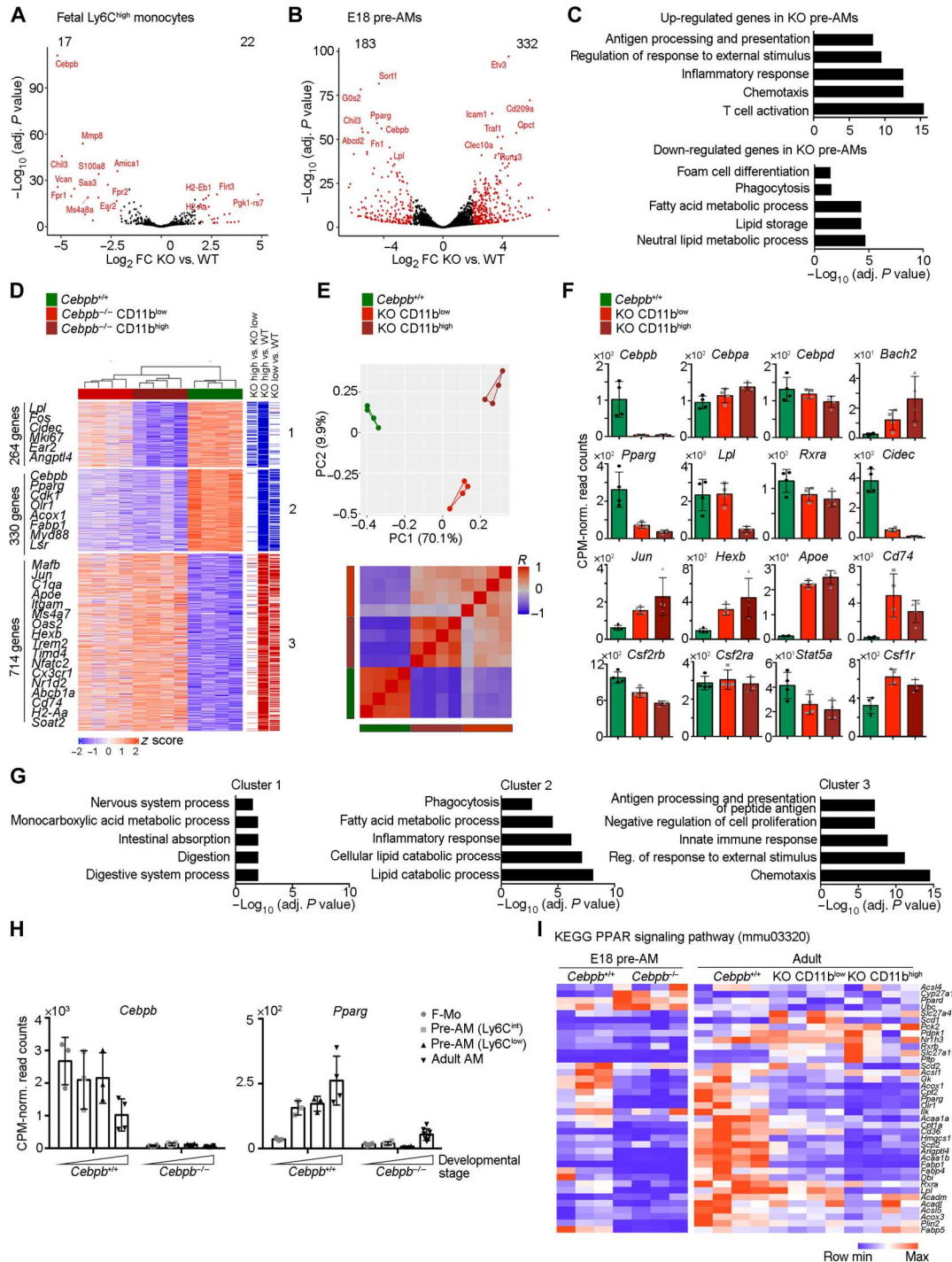


**Fig. 2. Transcriptomic analysis of embryonic and adult *Cebpb*-deficient AMs.** (A and B) Lung  $Ly6C^{high}$  F-Mo and lung  $Ly6C^{low}$  pre-AMs were FACS-isolated from *Cebpb*-proficient ( $n = 3$ ) and *Cebpb*-deficient ( $n = 4$ ) E18 mouse embryos and analyzed by RNA-seq. Depicted are all detected genes, with DEGs (adj.  $P < 0.01$  and  $|\log_2FC| > 2$ ) marked in red. (C) GO enrichment analysis of the DEGs between *Cebpb*-deficient and control pre-AMs. Shown are terms from the category “biological process.” (D) AMs from WT littermates and  $CD11b^{high}$  and  $CD11b^{low}$  AMs from adult *Cebpb*-deficient mice were isolated by FACS and analyzed by RNA-seq ( $n = 4$  mice per genotype). Shown are genes with an adj.  $P < 0.01$  and  $|\log_2FC| > 1$  in at least one pairwise comparison. Columns on the right hand of the heatmap indicate significantly differential genes in the indicated contrasts. Significantly up-regulated genes are marked in red, and significantly down-regulated genes are marked in blue. (E) PC analysis (top) and correlation matrix (bottom) of the three cell populations described in (D). (F) Normalized CPM read counts of AM genes of interest (means  $\pm$  SD). (G) GO enrichment analysis of the three clusters depicted in (D). Only biological process terms are shown. (H) Normalized CPM read counts of *Cebpb* and *Pparg* expression in F-Mo, pre-AM I ( $Ly6C^{int}$ ), pre-AM II ( $Ly6C^{low}$ ), and adult AMs isolated from WT and *Cebpb*-deficient mice. (I) Heatmap showing the expression of genes involved in the KEGG PPAR signaling pathway (mmu03320) in *Cebpb*-deficient and *Cebpb*-proficient E18 pre-AMs and adult AMs. Shown are only genes that were detected with  $>10$  reads in at least one group. See also data S1 for the full description of DEGs in F-Mo, pre-AMs, and adult AMs.



such as defects in immune response (up-regulated in *C/EBPβ* KO AMs) and lipid metabolism (down-regulated in *C/EBPβ* KO AMs), were inherent to *Cebpb*-deficient AMs irrespective of sex or housing conditions (fig. S2, C to F).

Because we observed the down-regulation of the key AM TF *Pparg* in *Cebpb*-deficient cells at the E18 pre-AM and adult stages, we explored the temporal sequence of *Cebpb* and *Pparg* expression in AMs. F-Mo was the earliest precursor stage investigated

and already expressed high levels of *Cebpb*, but the expression of *Pparg* only started to increase in  $Ly6C^{int}$  pre-AMs (Fig. 2H; gating strategy in fig. S1, C and D), which is in line with a previous report (5). Pre-AMs of *Cebpb*-deficient mice showed a strong reduction of *Pparg* transcripts (Fig. 2H). We furthermore analyzed the expression of genes involved in the Kyoto Encyclopedia of Genes and Genomes (KEGG) PPAR signaling pathway (mmu03320) in *Cebpb*-deficient and WT E18 pre-AMs and adult AMs (Fig. 2I).

Genes involved in the PPAR pathway were highly expressed in adult WT AMs and, to a lesser extent, also in their E18 precursors (Fig. 2I). The absence of C/EBP $\beta$  led to a deregulation of PPAR signaling-related genes in immature and adult *Cebpb*-deficient AMs (Fig. 2I). Our transcriptomic data suggest a critical regulatory role of C/EBP $\beta$  in the lipid metabolism and immune function of immature and mature AMs.

### C/EBP $\beta$ -deficient AMs are functionally impaired

The transcriptomic profile of adult CD11b<sup>low</sup> and CD11b<sup>high</sup> KO AMs indicated a functional impairment in their phagocytic and proliferative capacities. To corroborate this finding, we isolated AMs from C/EBP $\beta$  KO and WT littermates, incubated them with fluorescent beads, and examined bead uptake by flow cytometry. In contrast to WT AMs, both CD11b<sup>low</sup> and CD11b<sup>high</sup> C/EBP $\beta$  KO AMs showed compromised phagocytic activity (Fig. 3A). We then used the interferon (IFN) type I-inducible Mx-Cre system (16) to test whether the phagocytic impairment of AMs was directly C/EBP $\beta$  dependent or was due to a secondary effect of the observed

PAP phenotype and the accumulation of lipids in C/EBP $\beta$ -deficient lungs (Fig. 1D). AMs from Mx-Cre *Cebpb*<sup>fl/fl</sup> and Mx-Cre *Cebpb*<sup>+/+</sup> mice were isolated and cultured with CSF2 (Fig. 3B). After 7 days, cells were treated with IFN- $\alpha$  to induce Mx-Cre-mediated *Cebpb* deletion and were analyzed for phagocytic activity at day 14. As shown in Fig. 3C, Cre-induced deletion of *Cebpb* resulted in significantly reduced phagocytosis ( $P < 0.001$ ).

We next analyzed the proliferation capacity of C/EBP $\beta$  KO AMs. Isolated WT and C/EBP $\beta$  KO AMs were labeled with the fluorescent dye carboxyfluorescein succinimidyl ester (CFSE) and were cultured for up to 7 days in vitro in the presence of CSF2 to induce proliferation. The proportion of CFSE-negative cells was measured to detect proliferating cells. The fraction of CFSE-negative WT AMs increased from 0% (SD  $\pm$  0.1%) to 85% (SD  $\pm$  16.0%) by day 7, whereas the CFSE-negative cell fraction in C/EBP $\beta$  KO only reached 25% (SD  $\pm$  25.5%; Fig. 3D), indicating an impaired capacity for proliferation. Of note, CD11b<sup>low</sup> and CD11b<sup>high</sup> KO AMs could not be discriminated in this assay because up-regulation of CD11b expression was observed during in vitro culture of AMs. To

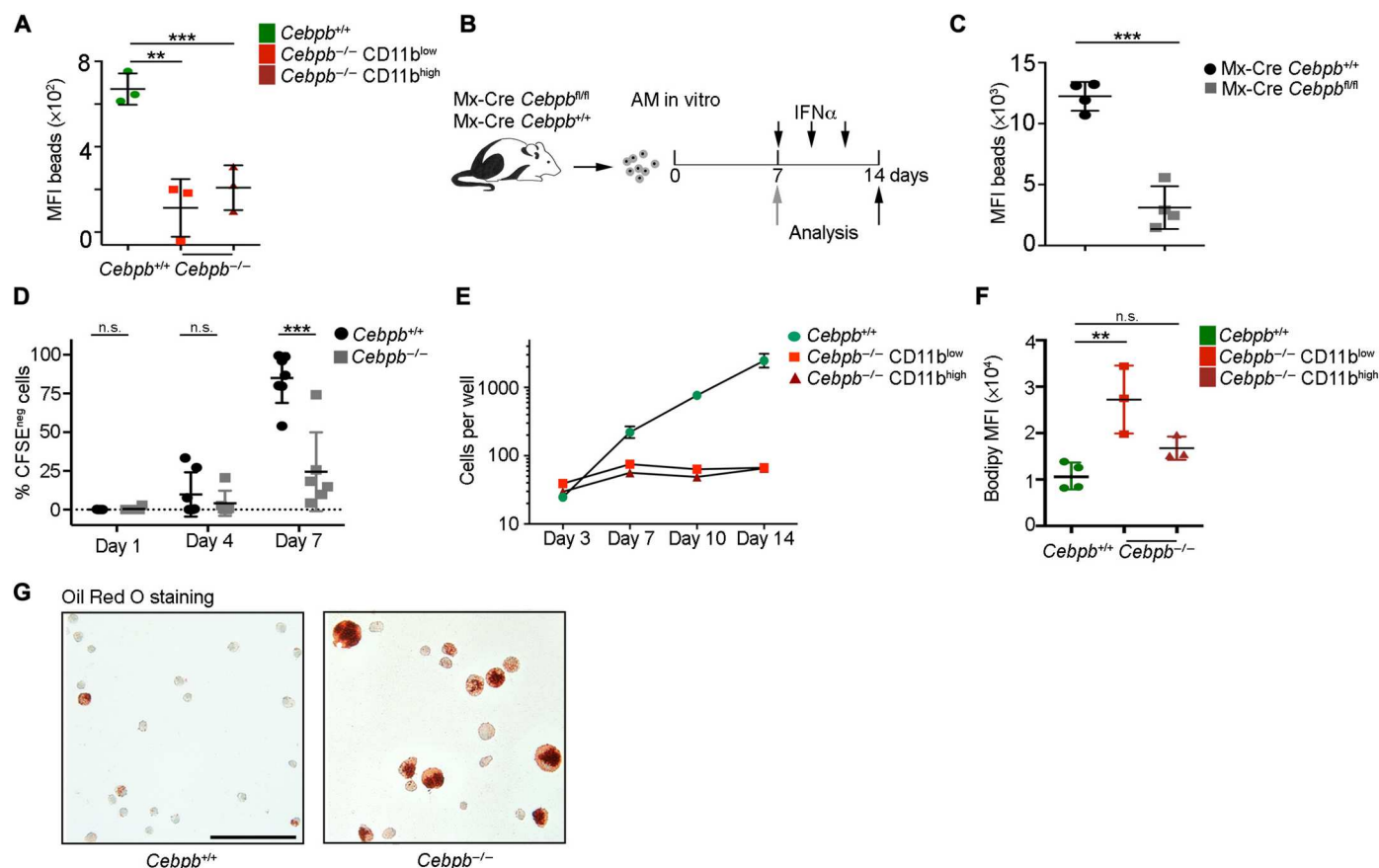


**Fig. 3. Functional impairment of adult *Cebpb*-deficient AMs.** (A) Latex bead phagocytosis of WT (green) and CD11b<sup>high</sup> (dark red) or CD11b<sup>low</sup> (light red) *Cebpb*<sup>-/-</sup> AMs was analyzed by flow cytometry. (B) Schematic of Mx-Cre experiment. BAL-isolated AMs were cultured with CSF2 for 7 days before IFN- $\alpha$  was added for a total of three times in 2-day intervals. Analysis was performed at day 14. (C) Latex bead phagocytosis of Mx-Cre *Cebpb*<sup>+/+</sup> control (black) and Mx-Cre *Cebpb*<sup>fl/fl</sup> AMs (gray). Shown is the MFI of phagocytosed beads as determined by flow cytometry. (D) CFSE analysis of WT and *Cebpb*<sup>-/-</sup> AMs. Cells were cultured for 1, 4, and 7 days with CSF2 and analyzed by flow cytometry. Quantification of CFSE<sup>neg</sup> cell frequency from two pooled experiments. (E) Quantification of in vitro cultured AMs. AMs from WT controls (green) and CD11b<sup>high</sup> (dark red) and CD11b<sup>low</sup> (light red) AMs from *Cebpb*<sup>-/-</sup> mice were sorted into 96-well plates in triplicates and cultured with CSF2. Cell numbers were tracked by microscopy at days 3, 7, 10, and 14 after seeding ( $n = 4$  mice per genotype). (F) WT (green) and CD11b<sup>high</sup> (dark red) and CD11b<sup>low</sup> *Cebpb*<sup>-/-</sup> (light red) AMs were loaded with Bodipy, and the MFI of Bodipy was analyzed by flow cytometry. (G) Oil Red O staining of WT (left) and *Cebpb*<sup>-/-</sup> AM (right) cytopins. Scale bar, 50  $\mu$ m. All experiments were performed twice with similar results ( $n = 2$  to 4 mice per genotype and experiment; means  $\pm$  SD).

investigate this point in more detail, we FACS-isolated WT and CD11b<sup>low</sup> and CD11b<sup>high</sup> C/EBPβ KO AMs, cultured them in the presence of CSF2, and tracked their cell numbers over the course of 2 weeks (Fig. 3E). We detected a steady increase in WT AMs, but both CD11b<sup>low</sup> and CD11b<sup>high</sup> C/EBPβ-deficient cells showed no change in cell numbers.

Last, because our transcriptomic analysis indicated defects in lipid metabolism in C/EBPβ KO AMs, we compared the intracellular lipid storage of AMs from C/EBPβ-deficient and C/EBPβ-proficient mice by Bodipy (Fig. 3F) and Oil Red O (Fig. 3G) staining. These assays revealed an accumulation of neutral lipids in both CD11b<sup>low</sup> and CD11b<sup>high</sup> mutant AMs. Together, these results demonstrate that the absence of C/EBPβ in AMs impairs their phagocytic and proliferative capacity in a cell-intrinsic manner and leads to a foamy macrophage phenotype.

### Key functional AM programs require cell-intrinsic expression of C/EBPβ

The C/EBPβ-dependent transcriptomic changes of AMs could either be AM-intrinsic effects or involve indirect mechanisms via other cells. To distinguish between these possibilities, we analyzed adult CD11c-Cre *Cebpb*<sup>fl/fl</sup> and LyzM-Cre *Cebpb*<sup>fl/fl</sup> mice, in which *Cebpb* is deleted in CD11c<sup>+</sup> cells or myeloid cells, respectively (17). Flow cytometric analysis revealed that CD11c-Cre *Cebpb*<sup>fl/fl</sup> mice had a similar phenotype to C/EBPβ KO mice with CD11b<sup>high</sup> cells and reduced cell numbers of BAL CD11b<sup>low</sup> AMs (fig. S3, A and B). Furthermore, the turbidity of BALF from CD11c-Cre *Cebpb*<sup>fl/fl</sup> mice was significantly increased compared with that of littermate controls ( $P < 0.001$ ; fig. S3C). Similar results were obtained for LyzM-Cre *Cebpb*<sup>fl/fl</sup> mice, which showed reduced AM cell numbers in BALF and lung tissue (fig. S3, D to F). However, both conditional KO lines showed an overall lower frequency of CD11b<sup>high</sup> AMs compared with C/EBPβ KO mice (Fig. 1A and fig. S3, A and D). The increase in BALF turbidity in either of the two Cre *Cebpb*<sup>fl/fl</sup> lines was also less pronounced than in C/EBPβ KO mice, indicating a milder phenotype (Fig. 1D and fig. S3, C and F).

Comparison of the transcriptomes of AMs from *Cebpb*<sup>-/-</sup>, CD11c-Cre *Cebpb*<sup>fl/fl</sup>, and LyzM-Cre *Cebpb*<sup>fl/fl</sup> mice and their respective controls by RNA-seq showed an overlap in the expression patterns between the different KO models. AMs from *Cebpb*<sup>-/-</sup> and LyzM-Cre *Cebpb*<sup>fl/fl</sup> mice clustered together in PC analysis (fig. S3, G and H, and data S2). We identified a cluster of genes that were up-regulated in all KO strains, including *Trem2*, *Cd74*, and *Abcb1a* (cluster 6), and genes in cluster 4 comprising *Pparg*, *Cebpb*, *Cidec*, and *Fabp1* were down-regulated in all *Cebpb*-deficient AMs (fig. S3, G to I). GO enrichment analysis revealed that cluster 6 was enriched for genes involved in the GO terms chemotaxis, inflammatory response, and immune effector process, whereas down-regulated genes in cluster 4 were enriched for lipid catabolic process, cell division, and sterol biosynthetic process (fig. S3J).

The transcriptional differences between the KO models, together with the potentially less severe PAP phenotype in the conditional mouse lines, may likely reflect the different promoter-dependent temporal onsets of *Cebpb* gene excision (7). *Cebpb* is highly expressed in pre-AMs and lung F-Mo and is required for the development of AMs from at least E18 onward (Figs. 1G and 2H). LyzM-Cre-mediated gene excision in AM precursor cells, however, only occurs around E18, and CD11c-Cre-mediated gene excision is

induced even later with the up-regulation of CD11c around P1 (7). Therefore, early C/EBPβ-dependent AM development is still unhindered in both conditional mouse lines, which may result in phenotypic variations between the three analyzed *Cebpb* KO models.

Collectively, these data demonstrate that C/EBPβ cell-intrinsically determines the transcriptomic programs of key AM functions such as lipid metabolism and antigen presentation. Additional C/EBPβ-dependent effects in nonmyeloid cells may further contribute to the phenotype observed in *Cebpb*<sup>-/-</sup> mice.

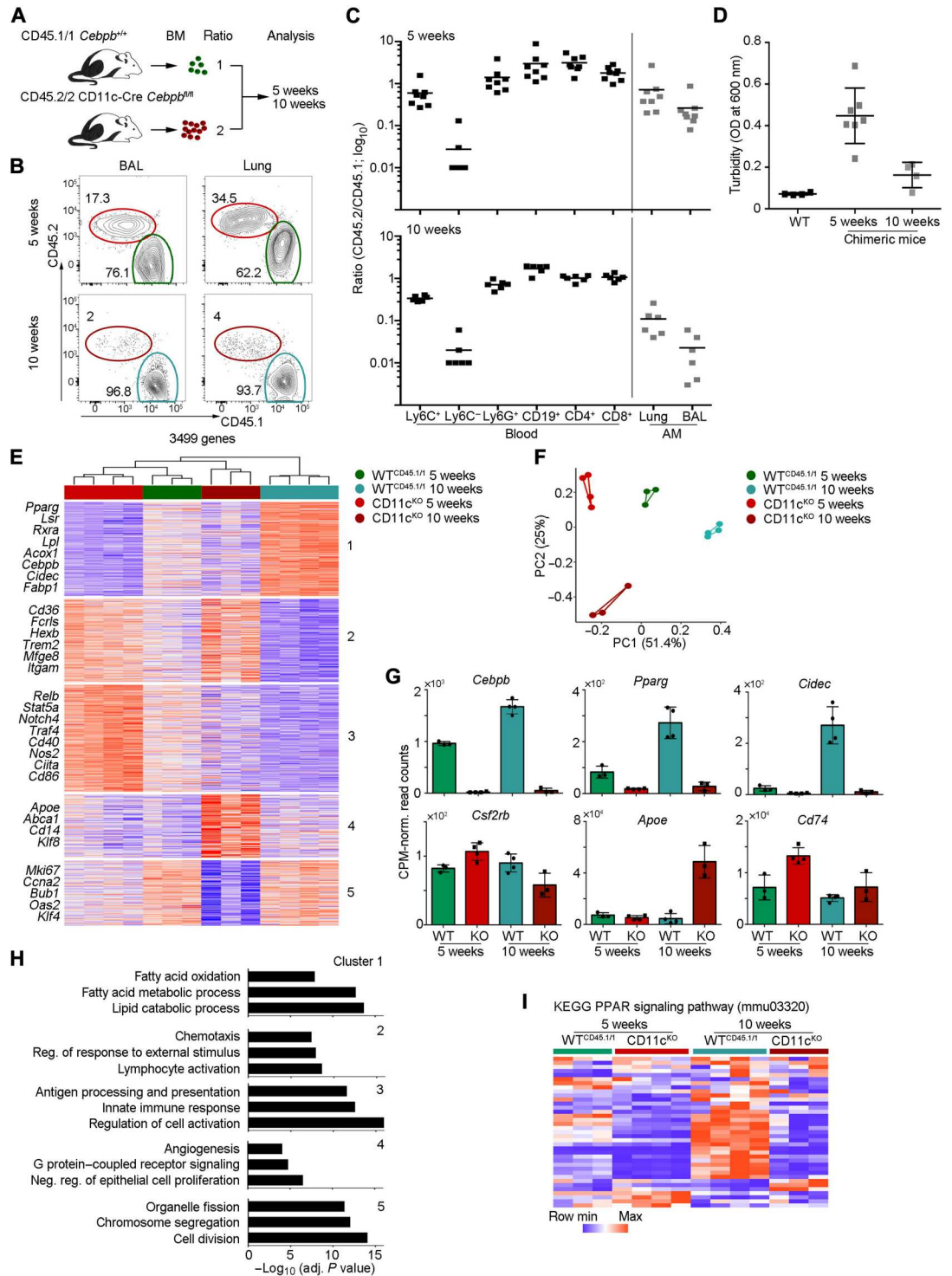
### C/EBPβ is required for the adaptation of monocytes to the AM niche after irradiation

Under specific conditions, such as inflammation or after lethal irradiation with BM transplantation, monocytes are able to adapt to a vacant alveolar niche and differentiate into functional AMs (3, 18). To examine whether C/EBPβ-deficient BM-derived cells can differentiate into AMs, we set up BM transplantation experiments in which CD45.1/1 WT BM cells were mixed with CD45.2/2 CD11c-Cre *Cebpb*<sup>fl/fl</sup> BM cells in a 1:2 ratio and injected into lethally irradiated CD45.1/2 recipients (Fig. 4A). Five weeks after BM transplantation, the ratio between CD45.2<sup>+</sup> CD11c-Cre *Cebpb*<sup>fl/fl</sup> and CD45.1<sup>+</sup> WT AMs in the lungs was similar to the ratio of reconstituted Ly6C<sup>high</sup> monocytes in the blood, which is indicative of a functional recruitment of *Cebpb*-deficient BM-derived cells to the lungs (Fig. 4, B and C). In agreement with the critical role of C/EBPβ in the development of monocytes (11), the Ly6C<sup>high</sup> and, to a much greater extent, the CD11c<sup>+</sup> Ly6C<sup>low</sup> monocyte compartment showed a lower ratio of CD11c-Cre *Cebpb*<sup>fl/fl</sup> to WT cells than lymphocytes (Fig. 4C). At 10 weeks after transplantation, CD45.2<sup>+</sup> CD11c-Cre *Cebpb*<sup>fl/fl</sup> lung and BAL AMs accounted for only a small fraction of the AM pool (2% SD ± 2%) and were almost completely outcompeted by WT cells. The BALF turbidity at 5 weeks was increased in C/EBPβ mixed chimeras, during which time *Cebpb*-deficient AMs were still present in the lungs. At 10 weeks after transfer, the turbidity normalized to control levels (Fig. 4D).

To gain information about the transcriptomic programs that regulate monocyte-to-AM differentiation, we performed bulk RNA-seq analysis at both time points using FACS-purified CD45.1<sup>+</sup> WT and CD45.2<sup>+</sup> CD11c-Cre *Cebpb*<sup>fl/fl</sup> lung AMs from the same recipient animals ( $n = 3$  to 4 per group; Fig. 4, E to G). We detected 3499 genes that were differentially expressed in at least one pairwise comparison (adj.  $P < 0.01$  and  $|\log_2FC| > 1$ ) and could be assigned to five clusters (Fig. 4, E to G). The expression of genes in cluster 1 increased from 5 to 10 weeks after transfer in CD45.1<sup>+</sup> WT AMs but was down-regulated in *Cebpb*-deficient cells at both time points. This cluster contained genes involved in the GO terms fatty acid oxidation and lipid catabolic process, such as *Pparg*, *Cidec*, and *Lsr* (Fig. 4, G and H). Genes that were specific to C/EBPβ KO AMs, independent of the isolation time point, could be detected in cluster 2 and were enriched for chemotaxis and lymphocyte activation. Genes involved in innate immune response and antigen processing and presentation were generally down-regulated from 5 to 10 weeks in both genotypes but were more highly expressed overall in C/EBPβ KO cells. The absence of C/EBPβ also affected genes related to cell division pathways at 10 weeks after transfer (cluster 5), which likely contributes to the competitive disadvantage of C/EBPβ KO cells. A more detailed analysis of the

**Fig. 4. C/EBPβ is required for the development of AMs from BM-derived cells after irradiation.**

**(A)** Schematic representation of BM transplantation experiment. **(B)** Exemplary flow cytometric analysis of BAL and lung AMs isolated from chimeric mice 5 and 10 weeks after BM transplantation. **(C)** Ratio of CD45.2<sup>+</sup> CD11c-Cre *Cebpb*<sup>fl/fl</sup> to CD45.1<sup>+</sup> WT leukocytes in the blood and lungs of recipient mice 5 weeks (top) and 10 weeks (bottom) after BM transfer. Shown are pooled data from two independent experiments with each having *n* = 3 to 5 mice per group. **(D)** Turbidity of BALF isolated from mixed BM chimeric mice and WT control animals as measured by the optical density at 600 nm. **(E)** CD45.1<sup>+</sup> WT (WT<sup>CD45.1/1</sup>) and CD45.2<sup>+</sup> CD11c-Cre *Cebpb*<sup>fl/fl</sup> (CD11c<sup>KO</sup>) donor-derived AMs were FACS-purified from the lungs of recipient mice 5 and 10 weeks after BM transplantation and subjected to RNA-seq analysis. Three or four animals per group were used. Shown are DEGs (adj. *P* < 0.01 and |log<sub>2</sub>FC| > 1 in at least one pairwise comparison) that were clustered in five groups. **(F)** PC analysis of the RNA-seq samples described in (E). **(G)** Gene expression examples of important AM genes. Shown are the means ± SD of CPM-normalized read counts. **(H)** GO enrichment analysis of the heatmap clusters depicted in (E). Only biological process terms are shown. **(I)** Expression of genes involved in the KEGG PPAR signaling pathway (mmu03320) in the AM groups described in (E). Shown are only genes that were detected with >10 reads in at least one group.



KEGG PPAR signaling pathway indicated that WT cells up-regulated genes involved in PPAR signaling from 5 to 10 weeks, whereas C/EBPβ-deficient BM-derived AMs were not able to induce the expression of this gene set, although the PAP phenotype and BALF turbidity were rescued by WT cells at 10 weeks after transfer (Fig. 4, D and I).

These data show that *Cebpb*-deficient BM-derived cells are not able to adapt to the lung environment after irradiation. These findings suggested that C/EBPβ is cell-intrinsically required for the establishment of the AM lipid metabolism machinery not only in embryo-derived AMs but also in BM-derived AMs.

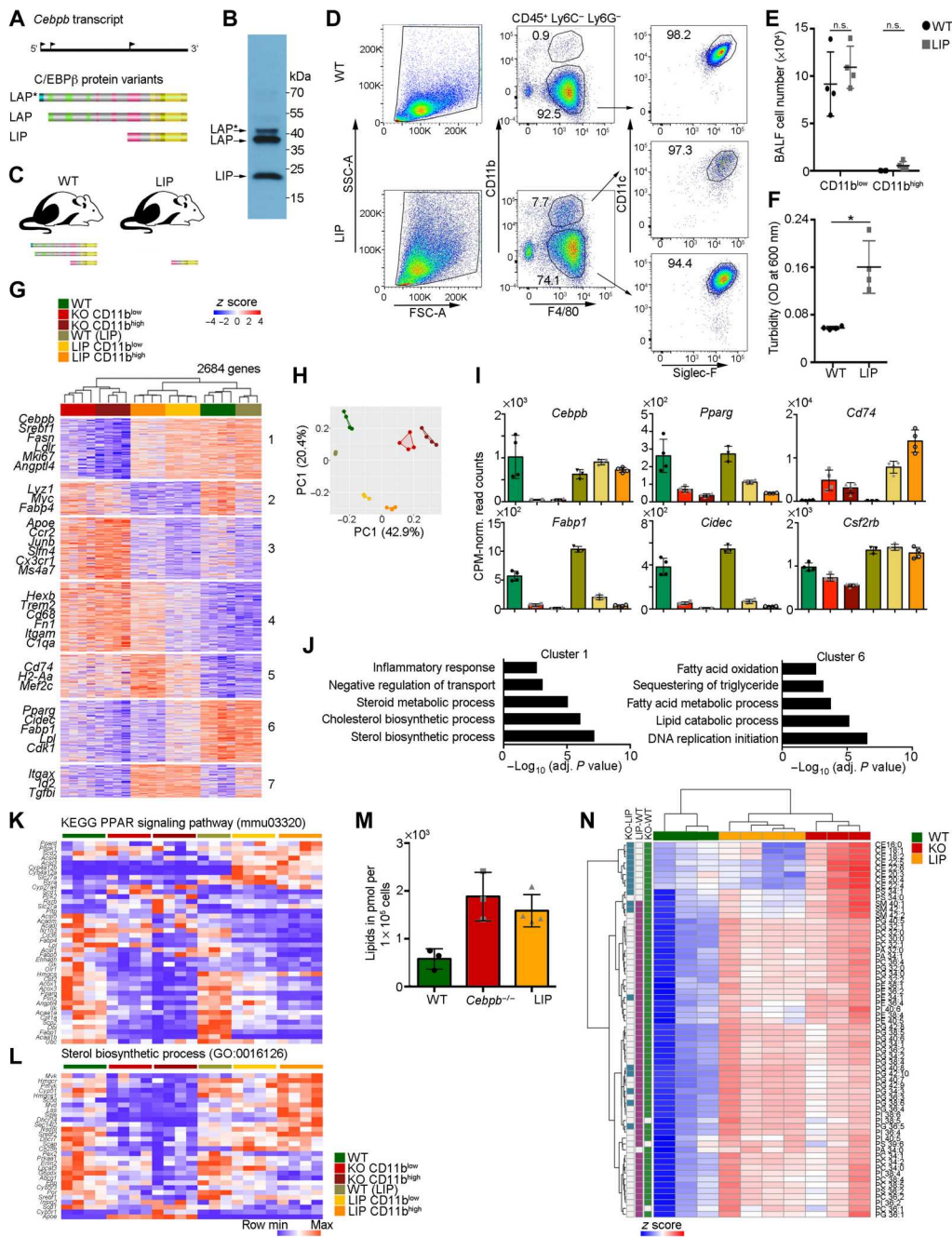
**The long C/EBPβ isoforms liver-enriched activating protein\* and liver-enriched activating protein are required for proper AM development**

The single-exon *Cebpb* gene can be translated into three different protein isoforms by differential usage of alternative start sites: liver-enriched activating protein\* (LAP\*), liver-enriched activating protein (LAP), and the short LIP isoform. The isoforms differ by the presence of a complex N-terminal transactivation domain (LAP\* and LAP) or its absence (LIP) (Fig. 5A) and have been shown to

be able to fulfill diverse and sometimes opposing functions in various regulatory settings (19). Under physiological conditions, AMs express all three C/EBPβ protein variants (Fig. 5B). To dissect the roles of the three C/EBPβ isoforms in the regulation of AMs, we analyzed the *Cebpb* mutant LIP mouse line, generated by a LIP knockin at the *Cebpb* locus and thus lacking the LAP\* and LAP sequence and expressing only the truncated LIP isoform (Fig. 5C) (20). BALF analysis of adult LIP (*Cebpb*<sup>LIP/LIP</sup>) mice by flow cytometry revealed phenotypic similarities to C/EBPβ KO mice, including

**Fig. 5. Partial rescue of the C/EBPβ-deficient phenotype by LIP expression.**

(A) Depiction of the different translational start sites of the *Cebpb* transcript and the resulting three alternative C/EBPβ protein variants. (B) Western blot analysis of C/EBPβ isoform expression in protein extracts of WT AMs from BALF. (C) Scheme of LIP mice, which harbor a knockin of the short C/EBPβ LIP isoform at the endogenous *Cebpb* locus. (D) Exemplary flow cytometric analysis of AMs isolated by BAL from homozygous LIP knockin mice (*Cebpb*<sup>LIP/LIP</sup>) and littermate controls. (E) Quantification of BAL AM cell numbers in LIP and control mice. (F) Turbidity of the BALF isolated from LIP mice and littermate controls as measured by the optical density at 600 nm. All experiments depicted in (D) to (F) were repeated at least twice ( $n = 4$  female mice per genotype and experiment; means  $\pm$  SD) with similar results. (G) CD11b<sup>high</sup> (orange) or CD11b<sup>low</sup> (yellow) LIP and littermate control (olive) AMs were sorted from BALF, analyzed by RNA-seq, and compared with *Cebpb*<sup>-/-</sup> AMs ( $n = 3$  or 4). The heatmap shows DEGs (adj.  $P < 0.01$  with  $|\log_2FC| > 1$  between at least two of the groups). See also data S3 for the full description of DEGs in adult LIP AMs. (H) PC analysis of the RNA-seq results with color code as in (G). (I) Gene expression examples of important AM genes. The means  $\pm$  SD of CPM-normalized read counts are shown. (J) GO enrichment analysis of cluster 1 (specifically down-regulated in *Cebpb*<sup>-/-</sup> AMs) and cluster 6 (commonly down-regulated in *Cebpb*<sup>-/-</sup> and LIP strains) of the heatmap shown in (G). Only biological process terms are shown. (K) Heatmap showing the expression of genes involved in the KEGG PPAR signaling pathway (mmu03320). Shown are only genes that were detected with  $>10$  reads in at least one group. (L) Heatmap showing the expression of genes involved in the GO pathway sterol biosynthetic process (GO:0016126). Shown are only genes that were detected with  $>20$  reads in at least one group. (M) Total amounts of membrane and storage lipids in  $1 \times 10^5$  FACS-isolated AMs from WT ( $n = 3$ ), *Cebpb*<sup>-/-</sup> ( $n = 3$ ), and LIP ( $n = 4$ ) mice. (N) Analysis of lipid types in AMs from WT (green), *Cebpb*<sup>-/-</sup> (red), and LIP (yellow) mice. Shown are lipids with  $P \leq 0.05$  as determined by Wilcoxon signed-rank test. The z score is based on  $\log_2$ -transformed picomoles per  $1 \times 10^5$  cell values.



Downloaded from https://www.science.org at Turku University on March 17, 2023

the presence of CD11b<sup>high</sup> AMs, although at lower frequency (Fig. 5, D and E, and Fig. 1, A and B). In contrast to C/EBP $\beta$  KO mice, the number of CD11b<sup>low</sup> AMs was not reduced in LIP mice (Fig. 5, D and E). Nevertheless, BALF turbidity was increased in these animals, indicating a functional impairment of AMs similar to that in C/EBP $\beta$  KO mice (Fig. 5F).

To compare AMs from C/EBP $\beta$  KO and LIP mice in more detail, we isolated AMs from LIP mice and WT control littermates ( $n = 3$  to 4 per genotype) and compared their transcriptomic profiles with those of C/EBP $\beta$ -deficient AMs. By pairwise comparisons of all analyzed populations, we detected 2684 DEGs (adj.  $P < 0.01$  and  $|\log_2 FC| > 1$ ) that were grouped in seven clusters (Fig. 5G and data S3). A large proportion of genes showed similar effects in LIP and KO AMs, including the down-regulation of genes involved in the GO terms fatty acid oxidation and lipid catabolic process (cluster 6), such as *Cidec*, *Fabp1*, and *Pparg*, and the up-regulation of genes related to major histocompatibility complex class II (MHCII) antigen presentation, such as *Cd74* and *H2-Aa* (cluster 5; Fig. 5, G to J). On the other hand, clusters 1 and 3 contained genes with an altered expression profile in KO but not in LIP AMs. Up-regulated genes specific to KO AMs (cluster 3) included genes related to antigen processing via MHC I and ion homeostasis, whereas cluster 1, with genes down-regulated specifically in KO AMs, was characterized by the GO terms cholesterol biosynthetic process and steroid metabolic process (Fig. 5J). Genes in clusters 2 and 7 that were differentially expressed between the KO and the LIP mouse strain showed no specific gene enrichment and could be attributed to the different genetic backgrounds of the two mouse lines (Fig. 5, G to J).

The common down-regulation of genes involved in fatty acid oxidation and lipid catabolic process was also apparent from a markedly disturbed expression of the KEGG PPAR pathway in both C/EBP $\beta$  mutant strains (Fig. 5K). In contrast, the expression of sterol biosynthetic process-related genes was partly rescued by LIP expression in vivo (Fig. 5L). To validate these findings, we compared the composition of storage and membrane lipids in WT and mutant AMs by lipidomic analysis using Orbitrap mass spectrometry. FACS-isolated AMs ( $1 \times 10^5$ ) from KO ( $n = 3$ ), LIP ( $n = 4$ ) (CD11b<sup>low</sup> and CD11b<sup>high</sup> AMs were pooled for both genotypes), and WT controls ( $n = 3$ ) were subjected to the analysis. Both KO and LIP AMs showed about threefold higher lipid content compared with WT cells (Fig. 5M). The major components of surfactant—namely, phosphatidylcholine, phosphatidylethanolamine, and phosphatidylglycerol—accumulated in both KO and LIP AMs. In line with the RNA-seq data, cholesterol esters were also enriched in *Cebpb*-deficient AMs, whereas their physiological concentrations were restored by LIP expression (Fig. 5N).

Together, these data show that the expression of the truncated C/EBP $\beta$  isoform LIP is not sufficient to overcome the C/EBP $\beta$ -dependent establishment of a PAP-like phenotype. However, LIP expression was found to rescue some of the C/EBP $\beta$  deficiency-mediated transcriptional changes in AMs, especially those related to sterol and cholesterol biosynthetic processes.

### DNA regions with RXRA:PPAR $\gamma$ motifs are less accessible in C/EBP $\beta$ -deficient AMs

To identify C/EBP $\beta$ -dependent DNA regions and uncover TFs that might cooperate with C/EBP $\beta$  and play a role in the observed AM phenotypes, we isolated BAL AMs and performed C/EBP $\beta$

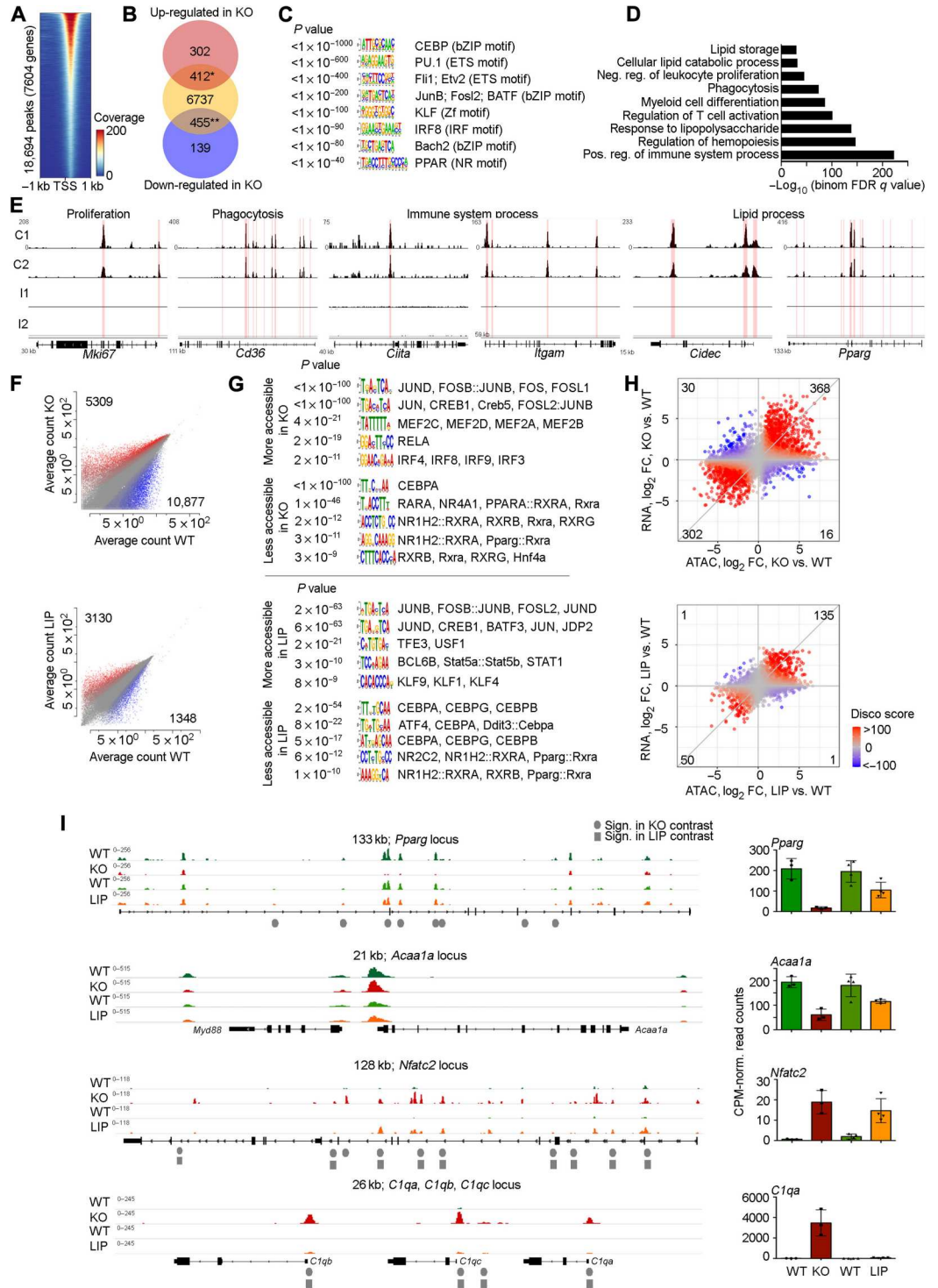
chromatin immunoprecipitation (ChIP)mentation (21). In comparison with input DNA control samples, C/EBP $\beta$  binding was detected at 18,694 DNA regions, which could be assigned to 7604 nearest genes (Fig. 6A). Most of the C/EBP $\beta$  binding events were located in close proximity to transcriptional start sites (TSSs) of genes (Fig. 6A). A comparison of the identified down- and up-regulated genes in *Cebpb*-deficient AMs by RNA-seq (Fig. 2D) with the 7604 genes that showed C/EBP $\beta$  binding revealed that 58% of the up-regulated genes ( $P = 1.1 \times 10^{-8}$ ) and 77% of the down-regulated genes ( $P = 2.2 \times 10^{-16}$ ) showed at least one binding event of C/EBP $\beta$  (Fig. 6B and data S4). These data indicate that C/EBP $\beta$  can function as a repressor or activator of gene expression. TF motifs that were present in DNA sequences within C/EBP $\beta$  binding peaks showed a significant enrichment of C/EBP and PU.1 motifs ( $P < 1 \times 10^{-1000}$  and  $P < 1 \times 10^{-600}$ , respectively; Fig. 6C). Motifs belonging to Ets2, JunB, KLF, and IFN regulatory factor (IRF) TFs, as well as PPAR motifs, were also evident in C/EBP $\beta$  binding sequences. GO enrichment analysis with all C/EBP $\beta$ -bound genes revealed that this set of genes was enriched for genes involved in immune system process, myeloid cell differentiation, phagocytosis, and lipid catabolic processes (Fig. 6, D and E, and fig. S4A).

To elaborate these findings in more detail, we performed chromatin accessibility analysis by transposase-accessible chromatin sequencing (ATAC-seq) (22) of FACS-isolated AMs from WT, *Cebpb*-deficient ( $n = 3$  per genotype), and LIP knockin animals ( $n = 4$  per genotype). In total, 16,186 differential peaks were detected in KO cells with  $|\log_2 FC| > 2$  and adj.  $P < 0.05$ , of which 5309 peaks (assigned to 2435 genes) indicated enhanced accessibility and 10,877 peaks (assigned to 4054 genes) were less accessible in KO AMs (Fig. 6F and data S5). The changes in LIP AMs were less pronounced compared with KO cells, and we detected 3130 peaks (assigned to 1421 genes) with a higher accessibility and 1348 peaks (assigned to 601 genes) that were less accessible in AMs isolated from LIP mice compared with littermates (Fig. 6F and data S6).

Next, we determined motif enrichment within the DNA regions corresponding to the differential peaks. Regions that were more accessible in KO and LIP AMs compared with WT cells were enriched for FOS and JUN motifs (Fig. 6G). *Cebpb* deficiency also led to more open chromatin regions with IRF, RELA, and nuclear factor  $\kappa$ B motifs, which is in agreement with the C/EBP $\beta$  ChIPmentation data. Peaks with decreased accessibility in both KO and LIP AMs were enriched for C/EBP and RARA/RXRA/Rxra:PParg motifs. The RNA expression levels of the identified TFs are depicted in fig. S4B. Similar results were obtained when we focused our analysis only on peaks in proximal TSS regions ( $\pm 3$  kb from TSS) instead of all detected peaks (fig. S4, C to E). When we compared the chromatin accessibility with the transcriptomic signature of the same samples, we observed many concordant changes (Fig. 6H). An increase in chromatin accessibility was generally accompanied by an increase in RNA expression of the corresponding gene and vice versa. However, a fraction of genes showed a discordant behavior, as described earlier (23). We identified genes such as *Pparg*, which showed ATAC-seq rescue by LIP that was not accompanied by transcriptomic rescue, indicating the requirement of the C/EBP $\beta$  transactivation domain for the induction of gene expression (Fig. 6I). Some genes, including *Acaa1a*, showed no ATAC-seq peak changes in *Cebpb* mutant cells compared with WT but had lower RNA expression. Moreover, the defects in *Nfatc2* could not be rescued on chromatin or RNA level by LIP expression. In

**Fig. 6. C/EBPβ-dependent epigenetic changes in AMs.**

**(A)** ChIPmentation analysis of the C/EBPβ-DNA binding in BAL-isolated WT AMs was performed in duplicates. Shown are the peak intensities and localization of C/EBPβ binding sites with respect to the closest TSS. **(B)** Overlap of the DEGs in *Cebpb*<sup>-/-</sup> AMs shown in Fig. 2D and the C/EBPβ-bound genes found in WT AMs. Significance was tested against a random set of genes with Fisher's exact test. \**P* = 1.1 × 10<sup>-8</sup> and \*\**P* = 2.2 × 10<sup>-16</sup>. See also data S4 for the full description of C/EBPβ-bound regions and overlapping genes. **(C)** Analysis of enriched TF motifs within C/EBPβ binding regions. Results are depicted as motif sequence with corresponding TF annotation and enrichment *P* value. **(D)** GO enrichment analysis of the 7604 genes assigned to C/EBPβ binding sites. FDR, false discovery rate. **(E)** Selected examples of gene loci involved in the indicated biological processes that show significant C/EBPβ binding (red areas) compared with input control. C, ChIP sample; I, input DNA sample. See also fig. S4A. **(F)** AMs from KO, LIP, and littermate controls were isolated by FACS and analyzed by ATAC-seq. Scatterplots showing the chromatin accessibility in the KO contrast (WT versus KO; top graph; *n* = 3 mice per genotype) and in the LIP contrast (WT versus LIP; bottom graph; *n* = 4 mice per genotype) depicted as the average read counts of all detected peaks. Colored dots correspond to significantly differential peaks (*q* < 0.05 and |log<sub>2</sub>FC| > 2; red, more accessible in mutant strain; blue, less accessible in mutant strain). **(G)** The differential peaks shown in (F) were used for motif enrichment analysis. Results are depicted as motif sequence with corresponding TF annotation and enrichment *P* value. Top: *Cebpb* KO contrast. Bottom: LIP contrast. **(H)** Disco plots showing the concordance between ATAC-seq and RNA-seq data. ATAC-seq peaks were assigned to genes according to their genomic location and their log<sub>2</sub>FC between WT and KO (top graph) and between WT and LIP (bottom graph) AMs were plotted against the log<sub>2</sub>FC of gene expression of the assigned gene as determined by RNA-seq analysis of the same AM samples. Genes with high concordance (determined by the disco score) are shown in red and genes with discordance in blue. For each quadrant, the number of concordant or discordant genes with |disco score| > 100 is indicated. **(I)** ATAC-seq IGV tracks of representative gene loci with corresponding gene expression (shown as CPM-normalized read counts; means ± SD) of the same AM samples as determined by RNA-seq. Gray circles indicate significant peak changes (*q* < 0.05 and |log<sub>2</sub>FC| > 2) in the KO contrast, and gray squares indicate significant peak changes in the LIP contrast. See also data S5 and S6 for a full list of accessible regions.



Downloaded from https://www.science.org at Turku University on March 17, 2023

summary, these data reveal that PPAR $\gamma$  motifs are present within many C/EBP $\beta$  binding regions and that RXRA:PPAR $\gamma$  motifs, in particular, were less accessible in the absence of C/EBP $\beta$ .

### **Cebpb- and Pparg-deficient AMs share transcriptomic alterations**

Our molecular analyses suggested an involvement of C/EBP $\beta$  in the regulation of PPAR $\gamma$  signaling in AMs. To further investigate this hypothesis, we compared the expression profiles of *Cebpb*-deficient AMs with published microarray data of AMs isolated from CD11c-Cre *Pparg*<sup>fl/fl</sup> mice that also develop PAP pathology (GSE60249) (7). Many of the DEGs (adj.  $P < 0.01$ ,  $|\log_2FC| > 1$ ) between AMs isolated from CD11c-Cre *Pparg*<sup>fl/fl</sup> animals and WT controls overlapped with those detected in both C/EBP $\beta$  KO populations compared with WT cells. In particular, CD11b<sup>high</sup> KO AMs clustered together with *Pparg*-deficient AMs in PC analysis (fig. S5, A to C). Many genes down-regulated in both C/EBP $\beta$ - and PPAR $\gamma$ -deficient AMs were genes involved in lipid metabolism, including *Fabp1*, *Lsr*, and *Cidec* (cluster 1; fig. S5, A and C). However, groups of PPAR $\gamma$  KO-specific and C/EBP $\beta$  KO-specific genes were also detected. Thus, the data indicate an involvement of C/EBP $\beta$  in *Pparg* signaling.

### **C/EBP $\beta$ -mediated induction of *Pparg2* requires CSF2**

Our analysis revealed that the phenotype of C/EBP $\beta$ -deficient AMs shared some resemblance with the phenotype observed in PPAR $\gamma$ <sup>-/-</sup> AMs. *Pparg* transcripts exist in two isoforms: Isoform 1 (*Pparg1*) is expressed across many cell types, whereas expression of isoform 2 is more restricted and especially reported for adipocytes (24). Another study demonstrated the expression of PPAR $\gamma$ 2 also in AMs (25). Because C/EBP $\beta$  is involved in the regulation of *Pparg2* during adipogenesis (26), we speculated that a similar mechanism might exist in AMs. Accordingly, we determined the expression of *Pparg1* and *Pparg2* in different TRM populations isolated from WT and *Cebpb*<sup>-/-</sup> animals by real-time quantitative polymerase chain reaction (qPCR) (Fig. 7A; gating strategies in fig. S1, F to I). We detected *Pparg1* transcripts in all investigated TRM subsets (Fig. 7A). In contrast, *Pparg2* expression was essentially restricted to AMs and only observed at a low level in white adipose tissue macrophages (WAMs). The absence of C/EBP $\beta$  led to a strongly reduced expression of *Pparg2* in AMs (32-fold decrease in KO), indicating that C/EBP $\beta$  is specifically involved in *Pparg2* regulation. Similar results were observed in AMs isolated from LIP animals (Fig. 7B), from CD11c-Cre *Cebpb* flox mice (Fig. 7C), and from BM-derived AMs 10 weeks after transplantation (Fig. 7D).

To examine whether C/EBP $\beta$  plays a pioneering or a constitutive role in *Pparg2* expression, we again took advantage of the IFN type I-inducible Mx-Cre system (16) as described earlier (Fig. 3B). *Cebpb* expression was detected in Mx-Cre *Cebpb*<sup>fl/fl</sup> AMs before IFN- $\alpha$  treatment at day 7 but was lost after IFN- $\alpha$  treatment at day 14 (Fig. 7E). At the same time, *Pparg2* expression significantly decreased in IFN- $\alpha$ -treated Mx-Cre *Cebpb*<sup>fl/fl</sup> cells, indicating that C/EBP $\beta$  is essential to maintain *Pparg2* expression in AMs. We used the same experimental setup to investigate the effect of IFN- $\alpha$ -induced C/EBP $\beta$  deletion on the *Pparg* chromatin status. After 7 days in culture, AMs from Mx-Cre *Cebpb*<sup>fl/fl</sup> ( $n = 3$ ) and Mx-Cre *Cebpb*<sup>+/+</sup> ( $n = 2$ ) mice were treated with IFN- $\alpha$  and harvested for ATAC-seq analysis at day 14. Loss of C/EBP $\beta$  in IFN- $\alpha$ -treated Mx-Cre *Cebpb*<sup>fl/fl</sup> AMs led to a significantly decreased accessibility

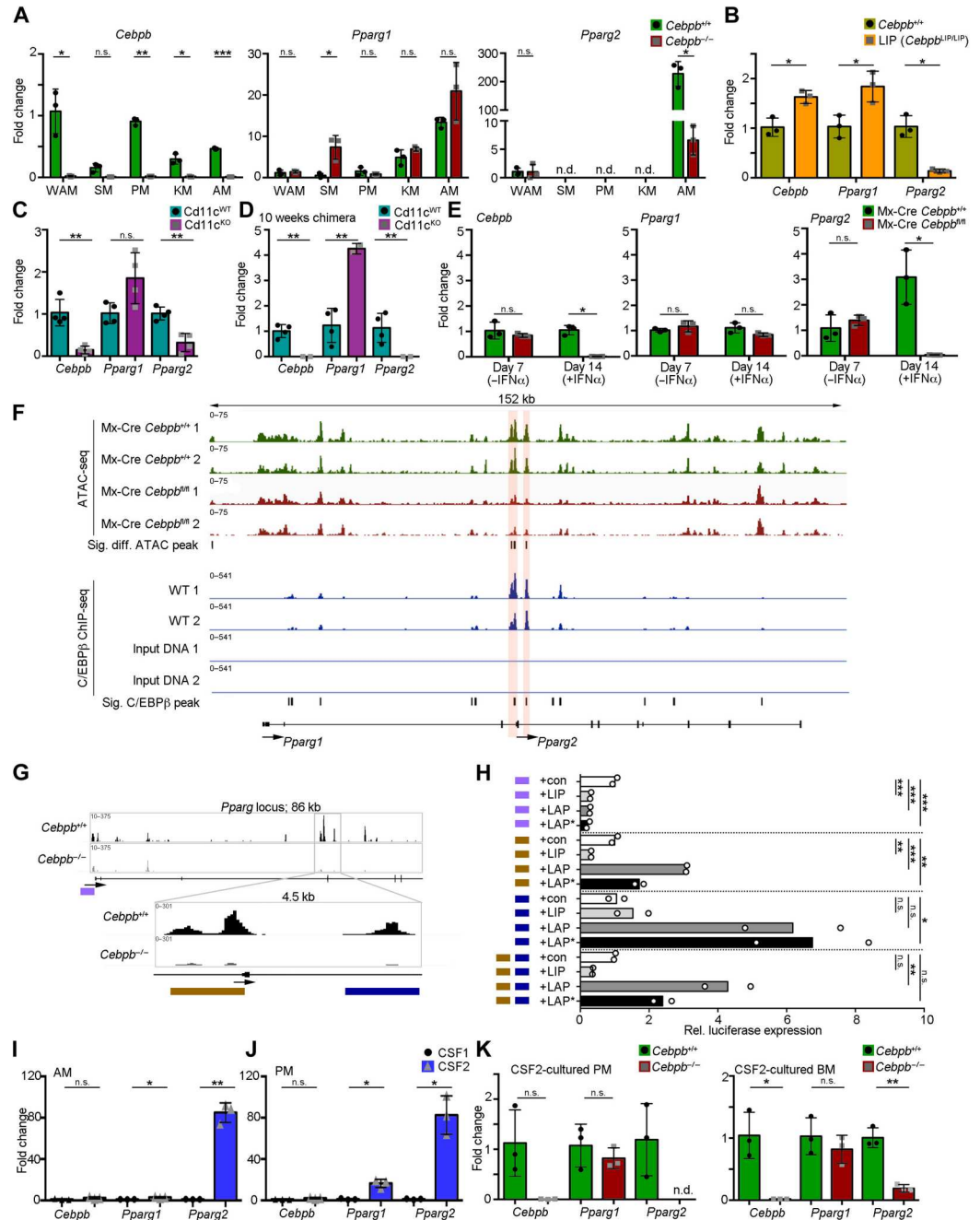
of the *Pparg2* locus, whereas other regions of the *Pparg* gene were not affected. The affected regions also showed strong C/EBP $\beta$  binding in our ChIPmentation data (Fig. 7F).

To confirm the regulatory sequences responsible for the C/EBP $\beta$ -mediated induction of *Pparg2* expression, we cloned the *Pparg1* and *Pparg2* promoter regions, as well as a *Pparg2* enhancer element, which showed C/EBP $\beta$  binding in WT AMs (Fig. 7, F and G), into a luciferase reporter vector. We transfected *Cebpb*-deficient mouse embryonic fibroblasts (MEFs) with the different promoter/enhancer constructs and introduced empty vector (con) or plasmids encoding one of the three C/EBP $\beta$  isoforms, LIP, LAP, or LAP\*. Measurement of the relative luciferase expression normalized to *Renilla* luciferase activity revealed that the *Pparg1* promoter was active independent of C/EBP $\beta$  isoforms, whereas the *Pparg2* promoter responded to the long C/EBP $\beta$  isoforms LAP and LAP\* but not to LIP (Fig. 7H). The *Pparg2* enhancer element, however, was even more responsive to the long C/EBP $\beta$  isoforms and was sufficient to activate luciferase expression.

Expression of *Pparg* in AMs was shown to be induced by CSF2; however, it was not discriminated between the different *Pparg* isoforms (7). Therefore, we next tested whether CSF2 is obligatory for *Pparg2* and *Cebpb* expression. We isolated WT AMs by BAL and cultured them either with CSF1 or CSF2 for 48 hours. Analysis by qPCR revealed that the expression of *Pparg2* was increased when AMs were treated with CSF2 as compared with cells cultured with CSF1 (85-fold SD  $\pm$  9.4), whereas *Cebpb* expression was unchanged (Fig. 7I). In line with this, inhibition of Janus kinase (JAK) 1 and JAK2, an established transducer of CSF2 signaling (27), by ruxolitinib prevented the CSF2-mediated induction of *Pparg2* but had only moderate effects on the expression of *Cebpb* (fig. S6A). These data indicate that CSF2 is mandatory for the continuous maintenance of *Pparg2* but not of *Cebpb* transcripts in AMs. To verify this finding in vivo, we analyzed the transcriptomic profiles of FACS-purified pre-AMs from *Csf2rb*-deficient E18 embryos and compared them with *Cebpb*-deficient pre-AMs (fig. S6, B to F, and data S7; gating strategy in fig. S1, C and D). Although both genotypes showed differences in *Pparg* expression and genes involved in lipid signaling, *Cebpb* itself was similarly expressed in WT and *Csf2rb*-deficient pre-AMs (fig. S6E). These data again demonstrate that CSF2 does not induce *Pparg2* by regulating *Cebpb* mRNA levels.

*Pparg* isoform expression analysis revealed the absence of *Pparg2* in PMs and other TRM populations (Fig. 7A). To test whether CSF2 can induce *Pparg2* also in these macrophage populations, we cultured PMs, which express high levels of *Cebpb* (Fig. 7A; immgen.org), with CSF1 or CSF2 for 48 hours. Treatment with CSF2 was able to induce *Pparg2* in PMs, whereas this isoform was barely detectable in CSF1-treated cells (83-fold SD  $\pm$  18.7 higher in CSF2-cultured cells; Fig. 7J). To investigate whether C/EBP $\beta$  is also involved in this CSF2-dependent induction of *Pparg2* in PMs, we isolated PMs from WT, C/EBP $\beta$  KO, and LIP mice by FACS and stimulated the cells with CSF2 for 48 hours. *Pparg2* expression was strongly diminished in *Cebpb*-deficient and LIP PMs (Fig. 7K and fig. S7A). Similar results were obtained for CSF2-cultured BM cells generated from C/EBP $\beta$  KO (Fig. 7K), CD11c-Cre *Cebpb* flox, and LIP mice (fig. S7, B and C). Collectively, our data show that the long C/EBP $\beta$  isoforms LAP and LAP\* can directly induce the expression of *Pparg2* in the presence of active CSF2 signaling.

**Fig. 7. C/EBPβ regulates Pparg2 expression in AMs.** (A) qPCR of *Cebpb*, *Pparg1*, and *Pparg2* mRNA expression in WAMs, spleen macrophages (SM), PM, kidney macrophages (KM), and AMs isolated by FACS from WT (green) and *Cebpb*-deficient mice (red). n.d., not detectable. Data are normalized to expression in WT WAM samples. (B to D) *Cebpb*, *Pparg1*, and *Pparg2* mRNA expression in AMs isolated by FACS from (B) LIP mice (orange) and controls (olive), (C) CD11c-Cre *Cebpb*<sup>fl/fl</sup> mice (CD11c<sup>KO</sup>, purple) and controls (CD11c<sup>WT</sup>, turquoise), and (D) CD11c-Cre *Cebpb*<sup>fl/fl</sup> (CD11c<sup>KO</sup>, purple) and CD11c-Cre *Cebpb*<sup>+/+</sup> (CD11c<sup>WT</sup>, turquoise) AMs isolated from mixed BM chimeras 10 weeks after transfer. Data are normalized to expression in the respective WT samples. (E) qPCR of *Cebpb*, *Pparg1*, and *Pparg2* expression in AMs isolated from Mx-Cre *Cebpb*<sup>fl/fl</sup> (red) and Mx-Cre *Cebpb*<sup>+/+</sup> control mice (green) was performed at day 7 (-IFN-α) and at day 14 (+IFN-α). For experimental scheme, see Fig. 3B. Data are normalized to expression in day 7 (-IFN-α) WT samples. (F) Top four IGV tracks: ATAC-seq data derived from day 14 IFN-α-treated Mx-Cre *Cebpb*<sup>fl/fl</sup> (*n* = 3) and control Mx-Cre *Cebpb*<sup>+/+</sup> AMs (*n* = 2; for experimental scheme, see Fig. 3B). Regions with significant changes in accessibility between the genotypes are indicated underneath the tracks. Bottom four IGV tracks: C/EBPβ binding as determined by CHIPmentation in WT AMs (*n* = 2). Input samples served as controls. Significant C/EBPβ-bound regions are indicated underneath the tracks. (G) Closer representation of ATAC-seq tracks of the *Pparg* locus in WT and *Cebpb*<sup>-/-</sup> AMs. Indicated are the *Pparg1* promoter (violet), *Pparg2* promoter (brown), and *Pparg2* enhancer (blue) regions used for luciferase reporter constructs. (H) *Cebpb* KO MEFs were transfected with *Pparg* promoter/enhancer pGL4.10 constructs [color code as in (G)] and received either control (con; pcDNA3.1) or *Cebpb* vectors (LAP\*, LAP, and LIP in pcDNA3.1). Shown is the FC of luciferase activity to control-treated cells. Mean with *n* = 2. Experiment was repeated twice. (I and J) *Cebpb*, *Pparg1*, and *Pparg2* expression in AMs and PMs cultured with CSF1 or CSF2 for 48 hours. Data are normalized to expression in CSF1 samples. (K) *Cebpb*, *Pparg1*, and *Pparg2* expression in PMs cultured with CSF2 for 48 hours (left) and CSF2-cultured BM-derived cells (right) isolated from *Cebpb*<sup>-/-</sup> (red) and control mice (green). Data are normalized to expression in WT samples. Data in (A) to (E) and (I) to (K) are shown as mean FC ± SD with *n* = 3 or 4 mice per genotype.



**DISCUSSION**

Here, we unravel the gene regulatory networks that are required for AM development and lipid metabolism, and thus for lung integrity, and identify C/EBPβ as a central player. We expand on previous studies that reported reduced AM cell numbers in C/EBPβ<sup>-/-</sup> mice (12) and show that the AM cell-intrinsic effects of C/EBPβ deletion result in a functionally compromised AM pool with defects in

proliferation, phagocytosis, and lipid metabolism, collectively resulting in a PAP-like syndrome.

The development and maintenance of AMs rely on the bioavailability of CSF2 (2). The strong dependency of AMs on CSF2 is probably unique within the macrophage compartment, because most other TRM populations except for intestinal macrophages (28) are largely unaffected by genetic deletion of *Csf2* or *Csf2rb* under

physiological conditions (29, 30). One of the reasons why CSF2 might be evolutionarily selected for its function on lung AMs is that CSF2 signaling induces the nuclear receptor *Pparg* (7). In adipocytes, PPAR $\gamma$  controls the expression of genetic networks involved in lipid metabolism, transport, and storage (31). The presence of high lipid and lipoprotein concentrations in the form of lung surfactant makes it plausible that similar functions of PPAR $\gamma$  are cell-intrinsically required in AMs to transport and metabolize ingested surfactant lipids. However, it is unlikely that CSF2 signaling induces *Pparg* expression without the cooperation of additional signals or TFs. During in vitro differentiation of preadipocytes, adipogenesis-supporting factors such as 3-isobutyl-1-methylxanthine or dexamethasone induce *Cebpb* expression (32), which, in cooperation with the glucocorticoid receptor, activates the expression of *Pparg2* (33). As a functional consequence, *Cebpb*-deficient mice show deficits in adipogenesis in vivo (34). Of note, *Pparg2* is sufficient to further drive adipogenesis in vitro, whereas *Pparg1* is not (35). In line with these data, we found that *Cebpb*-deficient AMs showed strongly reduced levels of *Pparg2*. Moreover, AMs lost the expression and chromatin accessibility of *Pparg2* after Mx-Cre-mediated deletion of *Cebpb* in vitro, indicating a continuous role of C/EBP $\beta$  for *Pparg2* induction. Similar to the situation in adipocytes (36), the C/EBP $\beta$  isoforms LAP\* and LAP, but not LIP, were able to interact with *Pparg2* promoter and enhancer elements, whereas *Pparg1* was inhibited by all C/EBP $\beta$  protein variants. In line with recent results reported for human monocyte-derived cells (37), expression of *Pparg2* was also induced in WT but not in *Cebpb*-deficient PMs or BM-derived monocytes cultured with CSF2. All three macrophage subsets are characterized by an open chromatin structure at the *Pparg2* promoter region (38, 39). C/EBP $\beta$  binding at these positions was described for adipocytes (40), CSF2-cultured BM-derived macrophages (39), and also AMs, as shown here, which indicates that C/EBP $\beta$  is important for the accessibility of the *Pparg2* locus. LIP animals likewise showed an accessible *Pparg2* promoter but failed to induce its gene expression. Because LIP lacks the C/EBP $\beta$  transactivation domain, but includes the DNA binding basic leucine zipper, the sole chromatin accessibility seems to be insufficient for *Pparg2* induction. However, our data also show that LIP was able to rescue some of the defects observed in C/EBP $\beta$ -deficient AMs, which is in agreement with a recent report showing that many functions of LIP are not only dominant negative in nature (41).

It was previously shown that C/EBP $\beta$  requires posttranslational phosphorylation to become an activator of adipogenesis (36). Because PMs express high levels of *Cebpb* and show an accessible *Pparg2* locus, but do not normally transcribe this specific isoform, it is possible that CSF2 signaling induces posttranslational modifications of C/EBP $\beta$  in macrophages that enable its function as an activator of *Pparg2*.

In macrophages, PPAR $\gamma$  was shown to be involved in anti-inflammatory processes during their inflammatory response (42, 43). However, these studies did not distinguish between PPAR $\gamma$ 1 and PPAR $\gamma$ 2 isoforms. Although *Pparg1* is expressed more widely among different TRM populations, we show here that the expression of *Pparg2* appears to be specific to TRM populations with high exposure to CSF2 and/or a lipid-rich environment such as AMs. This might reflect different properties of PPAR $\gamma$ 1 and PPAR $\gamma$ 2 in macrophage biology. In line with this notion, Vav-Cre *Pparg*<sup>fl/fl</sup> mice, in contrast to C/EBP $\beta$  KO mice, lack classical

CD11b<sup>low</sup> AMs almost completely (7), which might suggest that the expression of *Pparg1* in C/EBP $\beta$  KO AMs is sufficient to overcome some of the early functional defects observed in complete *Pparg*-deficient AMs.

Because our study mainly focused on C/EBP $\beta$  and its molecular actions, our data cannot fully dissect the functional differences between the two PPAR $\gamma$  isoforms. *Pparg* isoform-specific KO mice and isoform rescue experiments will be required to clarify the multifaceted roles of PPAR $\gamma$  in more detail. Another open question concerns the cellular origin of CD11b<sup>high</sup> C/EBP $\beta$  KO AMs. Studies suggest origin-dependent differences in the molecular and functional properties of embryo- and monocyte-derived TRMs after experimentally induced niche liberation (23, 44). Although our experiments do not identify the ontogeny of CD11b<sup>high</sup> C/EBP $\beta$  KO AMs, our data show lipid metabolism defects in *Cebpb*-deficient AM precursor cells, adult AMs, and monocyte-derived AMs. This argues for a dominant role of C/EBP $\beta$  in the establishment and regulation of AM lipid metabolism and identity independent of the cellular origin.

In summary, our data suggest C/EBP $\beta$  as a central player in PAP pathogenesis because of its function in macrophage lipid metabolism. The molecular mechanism of C/EBP $\beta$ -induced *Pparg2* expression may also be relevant for other pathologies where macrophages encounter high lipid concentrations and have to cope with lipid accumulation, such as obesity or atherosclerosis.

## MATERIALS AND METHODS

### Study design

The objective of this study was to investigate the functional and molecular role of C/EBP $\beta$  in AMs. We used different mutant *Cebpb* mouse models to isolate AMs at different developmental stages and examine the molecular and functional effects of C/EBP $\beta$  deficiency or specific C/EBP $\beta$  isoform expression on AMs. We used flow cytometry, transcriptomic analysis by RNA-seq and qPCR, epigenetic analysis by ATAC-seq and chromatin immunoprecipitation sequencing (ChIPmentation), lipidomics analysis, and functional assays. Numbers of sampling and experimental replicates are indicated in the figure legends. Sample sizes were chosen according to previous comparable studies conducted in our laboratory and animal availability. Adult mice in control and test groups were age-, background-, and sex-matched. For cell quantifications and in vitro cell cultures, both male and female mice were used, with no statistical differences between the sexes. Investigators were not blinded. Outliers were only excluded in bulk RNA-seq analyses on the basis of poor sample quality.

### Mice

The following mouse strains were used in this study: B6.Cg.129P2-C/EBPb tm1Pjf (*Cebpb*<sup>-/-</sup> mice) (45), B6.Cg.129P2-C/EBPtm1.2Acle (LIP mice) (20), B6.129P2-Lyz2tm1(cre)Ifo/J (LyzM-Cre mice) (46), B6.SJL-Ptprca-Pepcb/BoyJ (CD45.1/1 mice), C57BL/6J-Tg(Igax-cre,-EGFP)4097Ach/J (CD11c-Cre mice) (47), B6.Cg-Tg(Mx1-cre)1Cgn/J (Mx-Cre mice) (16), and B6.129S1-Csf2rbtm1Cgb/J (*Csf2rb*<sup>-/-</sup> mice) (29). BALB/cJ-Cebpbtm1.1Elgaz/J (*Cebpb*<sup>fl/fl</sup> mice) (48) backcrossed to C57BL/6 were crossed with the respective Cre lines. The C/EBP $\beta$ <sup>-/-</sup> and LIP mice were kept on a mixed genetic background because these strains are not viable on a C57BL/6 background. Animals between 7 and 16 weeks

of age were used for analysis unless stated otherwise. For the generation of BM chimeras, 8- to 12-week-old recipient mice (CD45.1/2) were lethally irradiated (950 rads). On the following day, the recipients were reconstituted with  $5 \times 10^6$  BM cells, which were a mixture of 33% WT (CD45.1/1) and 66% CD11c-Cre *Cebpb*<sup>fl/fl</sup> (CD45.2/2; CD11c<sup>KO</sup>) BM cells, by tail vein injection. The animals received an antibiotic treatment with enrofloxacin in their drinking water for 10 days after irradiation. BM chimeras were analyzed 5 and 10 weeks after transfer.

All mice were maintained in a specific pathogen-free (SPF), temperature-controlled ( $22^\circ \pm 1^\circ\text{C}$ ) mouse facility on a 12-hour light, 12-hour dark cycle at the Max-Delbrück Center, Berlin, Germany. Both tested facilities here (fig. S2, C to E) were of FELASA SPF standard. However, in facility 1, *Helicobacter* spp., *Rodentibacter* spp., and noroviruses were occasionally evident. Food and water were given ad libitum. Mice were fed a usual chow diet. All animal experiments have been approved by the LAGeSo in Berlin in accordance with international guidelines.

### Cell isolation and preparation

Adult mice were euthanized by CO<sub>2</sub> inhalation or intraperitoneal injection of 150 mg/kg of body weight of pentobarbital sodium (WDT). BALF was isolated by intratracheal instillation and withdrawal of five times of 1-ml phosphate-buffered saline (PBS) with 2 mM EDTA and 1% heat-inactivated fetal bovine serum (FBS; Gibco) unless indicated otherwise. The fluid was filtered through a 100- $\mu\text{m}$  mesh, and AMs were harvested by centrifugation. PMs were isolated by peritoneal lavage with PBS containing 2 mM EDTA and 1% heat-inactivated FBS (Gibco). For the isolation of other TRMs, mice were intracardially perfused with PBS before spleen, kidney, and visceral white adipose tissues were removed. The spleen was dissociated through a 100- $\mu\text{m}$  cell strainer, red blood cells were lysed with ACK, and the samples were washed and then used for staining. Kidney and white adipose tissues were minced and digested with collagenase type IV (1 mg/ml; Gibco) and deoxyribonuclease I (DNase I; 2 mg/ml; Roche) in RPMI medium at 37°C for 30 min while shaking. After digestion, the samples were homogenized through a 100- $\mu\text{m}$  cell strainer and washed, and white adipose tissue samples were stained. Kidney cell suspensions were subjected to density centrifugation with 40% Percoll (Sigma-Aldrich) at 700g and 14°C for 20 min with low acceleration and no brake before they were again washed and stained. For the isolation of BM cells, femur and tibia were removed and flushed with PBS containing 2 mM EDTA and 1% heat-inactivated FBS (Gibco). Samples were then subjected to red blood cell lysis before further processing.

E18 embryos from time-mated mice were euthanized by decapitation before their lungs were removed, minced, and digested with collagenase type IV (1 mg/ml; Gibco) and DNase I (2 mg/ml; Roche) in RPMI medium at 37°C for 30 min while shaking. After digestion, the samples were filtered through a 100- $\mu\text{m}$  mesh, washed, and stained.

### Flow cytometry and cell sorting

All cells were blocked with anti-CD16/32 (2.4G2) before staining, and antibodies against CD11b (M1/70), CD11c (N418), Siglec-F (E50-2440), F4/80 (BM8), CD64 (X54-5/7.1), CD115 (AFS98), Ly6C (HK1.4), Ly6G (1A8), CD3e (145-2c11), CD45 (30-F11), B220 (RA3-6B2), MHCII (IAb; AF6-102.1), Cx3cr1 (SA011F11),

Ter119, CD131 (JORO50), CSF2RA (698423), and NK1.1 (PK136) from BioLegend, eBioscience, and R&D Systems were used. Samples were flow-sorted using AriaI, AriaII, or AriaIII (BD Biosciences, BD Diva Software) cell sorters. Flow cytometry analyses were performed on Fortessa or LSRII (BD Biosciences, BD Diva Software) and analyzed with FlowJo software v.10.7.1 (BD Biosciences).

### Turbidity quantification of BALF

For turbidity quantification of BALF, 250  $\mu\text{l}$  of 5 ml of BALF was diluted with 250  $\mu\text{l}$  of PBS, and the optical density was measured at a wavelength of 600 nm.

### ELISA of SP-D

BAL was performed using 1 ml of PBS and spun down at 100g for 3 min to separate the fluid supernatant from the cells. Subsequently, the supernatant of *Cebpb* KO samples was diluted 1:2500, and that of WT samples was diluted 1:1000 in PBS. ELISA was performed using a Systems Quantikine ELISA kit for mouse SP-D (R&D Systems) according to the manufacturer's protocol.

### May-Grünwald-Giemsa and Oil Red O staining

AMs were isolated by BAL and subjected to a Ficoll centrifugation to remove debris and dead cells. Cytospins were performed at 500 rpm with low acceleration for 5 min. For May-Grünwald-Giemsa stainings, cytospins were fixed in methanol for 5 min and stained with May-Grünwald solution for 5 min. Subsequently, the samples were washed with water and stained with a 5% Giemsa solution for 45 min before they were again washed with water. For Oil Red O stainings, cytospins were fixed in 4% paraformaldehyde (PFA) for 15 min, washed with PBS, rinsed with 60% isopropanol, and then stained in a 0.3% Oil Red O (Sigma-Aldrich) solution in 60% isopropanol for 60 min. The slides were again rinsed with 60% isopropanol, stained with hematoxylin (AppliChem) for 50 s, and washed with water.

### Phagocytosis assay

AMs were isolated by BAL and seeded in RPMI complete medium [RPMI 1640 GlutaMAX supplemented with 10% FBS (Gibco), 1% sodium pyruvate (Gibco), and 1% penicillin-streptomycin (Gibco)] in a non-tissue culture-treated six-well plate. The cells were incubated at 37°C for 2 hours to allow them to adhere. Next, the cells were incubated with or without fluorescent latex beads (Sigma-Aldrich) for 90 min either at 37°C or on ice. Afterward, they were washed with PBS three times, detached with trypsin, stained with surface marker antibodies, and analyzed by flow cytometry. To correct for unspecific adherence of the beads to the outside of the cells, the median fluorescence intensity (MFI) of bead-positive cells was calculated as follows: MFI of bead-positive cells incubated at 37°C – MFI of bead-positive cells incubated on ice.

### CFSE in vitro cell proliferation assay

AMs were isolated by BAL, resuspended in PBS with 5  $\mu\text{M}$  CFSE (BioLegend), and incubated at 37°C for 20 min to label the cells. After incubation, staining was quenched by adding five times the staining volume of RPMI complete medium. The cells were pelleted and seeded in RPMI medium in non-tissue culture-treated six-well plates. AMs were then incubated at 37°C for 4 hours to allow them to adhere before nonadherent cells were removed and the medium

was replaced by RPMI complete with CSF2 (20 ng/ml) (STEMCELL Technologies). AMs were cultured for up to 7 days, and every 2 to 3 days, the medium was replaced. On days 1, 4, and 7, fractions of the cells were harvested by trypsinization, stained with surface marker antibodies, and analyzed by flow cytometry.

### Bodipy staining

Freshly BAL-isolated AMs were stained with surface marker antibodies for flow cytometry before half of each sample was incubated in a 1:500 Bodipy 493/503 (Thermo Fisher Scientific) dilution in PBS at 37°C for 15 min. The other half of each sample was resuspended in a 1:500 dilution of dimethyl sulfoxide in PBS as controls. All samples were washed with PBS three times and analyzed by flow cytometry.

### Basic lipidomic analysis

For lipidomic analysis,  $1 \times 10^5$  AMs were sorted from BALF and frozen in liquid nitrogen. Quantitative analysis of lipids was performed by Lipotype GmbH, Dresden ([www.lipotype.com](http://www.lipotype.com)) according to their standard "basic lipidomics analysis" procedure using the Lipotype Shotgun Lipidomics technology together with high-resolution Orbitrap mass spectrometry.

### RNA isolation and cDNA synthesis for RNA-seq and real-time qPCR

Cells (500 to 20,000 sorted cells for RNA-seq) were lysed with 50 to 200  $\mu$ l of lysis/binding buffer (Life Technologies), frozen on dry ice, and stored at  $-80^\circ\text{C}$  until further use. The mRNA was purified using a Dynabeads mRNA DIRECT purification kit (Life Technologies) according to the manufacturer's guidelines. Reverse transcription was performed with oligo(dT) primers (Thermo Fisher Scientific) or MARS-seq barcoded RT primers and the AffinityScript cDNA (complementary DNA) Synthesis Kit (Agilent).

### Bulk RNA-seq

Bulk RNA-seq was performed according to a modified protocol of the original MARS-seq protocol (49, 50). Briefly, mRNA was subjected to reverse transcription using an AffinityScript cDNA synthesis kit (Agilent) and MARS-seq barcoded RT primers. Samples were analyzed by qPCR and pooled according to their Ct values. Pooled samples were treated with exonuclease I [New England Biolabs (NEB)] and size selected by a 1.2 $\times$  AMPure XP beads (Beckman Coulter) cleanup. Second-strand synthesis of the cDNA was performed using a second-strand synthesis kit (NEB). Afterward, samples were subjected to *in vitro* transcription with a HiScribe T7 RNA polymerase kit (NEB). The DNA template was removed by Turbo DNase I (Life Technologies) treatment. Subsequently, the RNA was fragmented at 70°C using RNA fragmentation buffer (Invitrogen), and samples were purified by 2 $\times$  SPRI cleanup. Afterward, fragmented RNA ligation with MARS-seq ligation adapter was performed with T4 RNA ligase (NEB). In a second reverse transcription reaction using the MARS-seq RT2 primer and an AffinityScript cDNA synthesis kit (Agilent Technologies), the RNA was transcribed into cDNA. As a final step, the library was amplified in a nested PCR with P5\_Rd1 and P7\_Rd2 primers and Kapa HiFi Hotstart ready mix (Kapa Biosystems) and purified with a 0.7 $\times$  AMPure XP beads cleanup. Library sizes and DNA concentration were determined using TapeStation (Agilent

Technologies) and a Qubit fluorometer (Life Technologies). The samples were sequenced using a NextSeq 500 system (Illumina).

### ATAC sequencing

For the preparation of ATAC-seq libraries, 15,000 to 20,000 cells were used (22) as described earlier (51). Briefly, nuclei were isolated by lysis with cold lysis buffer and centrifuged for 25 min at 500g and 4°C with low acceleration and brake using a swing-out rotor. The supernatant was carefully removed, and nuclei were resuspended in 25  $\mu$ l of reaction buffer containing 2  $\mu$ l of Tn5 transposase and 12.5  $\mu$ l of TD buffer (Nextera DNA library preparation kit, Illumina). The mix was incubated at 37°C for 1 hour. Afterward, the DNA was purified by adding 5  $\mu$ l of cleanup buffer, 2  $\mu$ l of proteinase K (NEB), and 2  $\mu$ l of 5% SDS. After an incubation phase of 30 min at 40°C, the tagmented DNA was enriched using AMPure XP beads (Beckman Coulter). The DNA was PCR-amplified with indexed primers and Kapa HiFi Hotstart ready mix (Kapa Biosystems). After the PCR, tagmented DNA fragments were selected for fragments smaller than 600 base pairs (bp) and purified using AMPure XP beads. Libraries were subjected to a second PCR amplification with Kapa HiFi Hotstart ready mix (Kapa Biosystems), indexing primers, and an appropriate number of reaction cycles depending on the library concentration. Library sizes and DNA concentration were determined using TapeStation (Agilent Technologies) and a Qubit fluorometer (Life Technologies). Libraries were sequenced with an average of 20 million reads per sample on a NextSeq 500 system (Illumina).

### ChIPmentation

Preparation of ChIPmentation samples was performed according to (21). AMs ( $2 \times 10^6$ ) were BAL-isolated from C57BL/6 mice and fixed in a 1% PFA solution (in 10% FBS/PBS). The fixation reaction was quenched on ice by addition of glycine (125 mM final concentration), and the samples were centrifuged at 300g for 5 min at 4°C. Subsequently, cell pellets were washed twice with cold PBS and 1 $\times$  protease inhibitor (Roche), snap-frozen in liquid nitrogen, and stored at  $-80^\circ\text{C}$  until further processing. The samples were thawed on ice and resuspended in chromatin prep buffer (High Sensitivity Chromatin Preparation kit, Active Motif) with 1 $\times$  protease inhibitor (Roche) before nuclei were released using a Dounce homogenizer with a tight pestle (Active Motif) and centrifuged at 4°C and 1250g for 5 min. Nuclei were then resuspended in cold sonication buffer and pipetted to facilitate nuclei disruption. The chromatin was sonicated using a Diagenode Bioruptor to achieve a fragment size ranging from 200 to 500 bp. One percent of the sonicated chromatin was used for the input sample; the rest was incubated overnight with prewashed A Dynabeads (Thermo Fisher Scientific; previously blocked with 0.1% bovine serum albumin) and 4  $\mu$ g of anti-C/EBP $\beta$  antibody (C-19; Santa Cruz Biotechnology). The following day, the beads were washed twice with RIPA-LS, twice with RIPA-HS, twice with RIPA-LiCl, and twice with 10 mM tris-HCl (pH 8.0) and resuspended and incubated in the tagmentation solution (0.25% tagmentation buffer and 2 mM Tn5; Illumina) for 2 min at 37°C. The tagmentation reaction was stopped on ice by adding cold RIPA-LS. Later, beads were washed twice in RIPA-LS and twice in 1 $\times$  TE and lastly resuspended in ChIP elution buffer. Samples were decross-linked overnight and purified on the following day using AMPure XP beads (NEB). Libraries were amplified using KAPA HiFi Hotstart ready mix (Kapa Biosystems)

with published indexing primers (22) and purified using AMPure XP beads (NEB). Library sizes and DNA concentration were determined using TapeStation (Agilent Technologies) and a Qubit fluorometer (Life Technologies). Libraries were sequenced with an average of 30 million reads per sample on a NextSeq 500 system (Illumina). The experiment was performed in duplicates.

### Processing and analysis of ATAC-seq data

ATAC-seq reads were aligned to the mouse genome v. GRCm38 using the BWA-MEM algorithm implemented in the bwa program, v.0.7.17 (52). Peaks were called with MACS2, v.2.2.7.1 and processed with the R package DiffBind (v.2.14) (53, 54). Differential binding analysis was performed using the DESeq2 R package (v.1.26) (55). ChIPseeker v.1.22.1 was used for peak annotation (56). For each comparison, significant peaks were defined as those with  $|\log_2FC| > 2$  and  $\text{adj. } P < 0.05$ . For motif search and annotation, the MEME suite (v.5.0.5) was used. Motifs were first identified using DREME by comparing differential peak sequences with background sequences separately for up- and down-regulated peaks. Then, identified motifs were annotated using the TOMTOM program and the Jaspar2020 database (57). For comparison between RNA-seq and ATAC-seq data, the R package disco (v.0.6) (58) was used to calculate the “disco score,” a heuristic metric based on  $P$  values and  $\log_2FC$  in both comparisons. Disco score takes extreme values for features that are either significantly regulated in the same direction in both comparisons (“concordant” features) or significantly regulated in opposite directions in the two comparisons (“discordant” features).

### Processing and analysis of RNA-seq and microarray data

We used FastUniq (59) to collapse PCR duplicates and STAR v2.6.1a (60) to align unique reads to the mouse genome (GRCm38). Gene expression was quantified using featureCounts v1.6.3 (61) and the Gencode vM12 reference. We then used DESeq2 v1.24 (55) on selected sample groups to perform differential expression between all pairs of conditions, with  $\text{ashr}$  shrinkage (62). Genes with  $\text{adj. } P < 0.01$  and  $|\log_2FC| > 1$  were selected, and  $z$  scores of  $\log_2$  counts per million (CPM) values were computed to construct a heatmap with ComplexHeatmap v2.0.0 (63), perform PC analysis, and cluster genes using  $k$ means. Gene set enrichment using gene sets from GO and KEGG was performed for each cluster with ClusterProfiler v3.12 (64) using all genes with mean CPM  $> 1$  as background.

For fig. S5, we downloaded the microarray data of CD11c-Cre *Pparg* flox and control AMs from Gene Expression Omnibus (GEO) (GSE60249) using the GEOquery package and averaged expression values over all probes for a given gene. We then combined  $\log_2(1 + \text{CPM})$  values from RNA-seq with microarray expression values, removing a batch effect between RNA-seq and microarray data with ComBat (65) after quantile normalization restricted to the intersection of the top 95% of genes from each dataset. We then performed differential expression analysis between pairs of conditions using limma v3.40.6 (66).

### Processing and analysis of ChIPmentation data

ChIPmentation data were analyzed with the Pigx pipeline for ChIP-seq data, which comprised a read trimming with Trim Galore, read mapping to mm10 with Bowtie2, and peak calling done by MACS (53, 54). We filtered the resulting peaks by false discovery rate with a

cutoff of  $1 \times 10^{-5}$  and merged them using DiffBind (53, 54) while retaining only those peaks found in both samples. This resulted in 18,694 peaks annotated with 7604 genes using GREAT. A coverage map of the 18,694 peaks was prepared with deeptools. We overlapped the annotated ChIP genes with genes deregulated in WT versus *Cebpb*-deficient adult AMs (Fig. 2D). To assess the significance of overlaps shown in the Venn diagram (Fig. 6B), we applied Fisher’s test.

### Western blot

AMs were isolated by BAL and lysed with RIPA buffer supplemented with  $1 \times$  cOmplete ULTRA protease inhibitor cocktail (Roche) and 1 mM dithiothreitol for 10 min on ice. Subsequently, protein lysates were sonicated in an ultrasonic water bath for 20 s and centrifuged at 14,000 rpm and 4°C for 10 min. The supernatant was transferred to a new tube and incubated with SDS loading buffer at 95°C for 5 min before proteins were separated by electrophoresis on a 4 to 15% Criterion TGX precast gel (Bio-Rad) at 100 to 130 V in SDS running buffer. Proteins were blotted onto a nitrocellulose membrane using the Trans-Blot Turbo System (Bio-Rad) at 2.5 A and 25 V for 10 min, and the membrane was blocked in milk Tris-buffered saline with Tween 20 (TBS-T) for 1 hour. After overnight incubation at 4°C with a 1:500 dilution of rabbit anti-C/EBP $\beta$  (C-19; Santa Cruz Biotechnology) antibody in milk TBS-T, the membrane was washed with TBS-T four times for 5 min and incubated with secondary antibody solution [1:5000; ECL anti-rabbit immunoglobulin G (GE Healthcare) in milk TBS-T] for 1 hour at room temperature. The membrane was again washed with TBS-T four times for 5 min before protein signals were detected using Immobilon Western chemiluminescent horseradish peroxidase substrate (Millipore).

### Real-time qPCR

qPCR of mouse cDNA was performed using the PowerUp SYBR Green Mastermix (Thermo Fisher Scientific) and the following primers: *Actb* (5'-GGAGATTACTGCTCTGGCTCC-3' and 5'-AGGGTGTAAAACGCAGCTC-3'), *Cebpb* (5'-TCGGGACTTGATGCAATCC-3' and 5'-AAACATCAACAACCCCGC-3'), *Pparg1* (5'-AAGAAGCGGTGAACCACTGA-3' and 5'-GGAATGCGAGTGGTCTTCCA-3'), and *Pparg2* (5'-TCGCTGATGCACTGCCTATG-3' and 5'-CGAGTGGTCTTCATCACGG-3'). Reactions were performed in 10- $\mu$ l reaction volumes on a QuantStudio 6 Flex real-time PCR system (Thermo Fisher Scientific). All analyzed expression levels were normalized to *Actb* expression.

### In vitro culture and treatment of Mx-Cre AMs

AMs were isolated by BAL, seeded in RPMI complete medium in non-tissue culture-treated 12-well plates, and incubated at 37°C to allow the AMs to adhere. After 4 hours, the medium was exchanged to remove nonadherent cells. AMs were cultured in RPMI complete medium supplemented with CSF2 (20 ng/ml; STEMCELL Technologies) for 7 days to expand the cells. Every 2 to 3 days, the medium was replaced. At day 7, a fraction of the AMs was harvested for analysis, whereas the remaining cells were treated with mouse IFN- $\alpha$  (1000 U/ml; Miltenyi) to induce Cre-mediated recombination. IFN- $\alpha$  treatment was repeated twice in 2-day intervals (see Fig. 3B). At day 14, all cells were harvested for analysis.

### In vitro culture of BM cells, PMs, and AMs

BM cells were flushed from femur and tibia and washed, and red blood cells were lysed. Cells ( $2 \times 10^5$ ) were resuspended in 1.5 ml of RPMI complete medium supplemented with CSF2 (20 ng/ml; STEMCELL Technologies), and cells were cultured in non-tissue culture-treated six-well plates. Every second day, the medium was exchanged. At day 7, cells were harvested, centrifuged, lysed with RNA lysis buffer (Life Technologies), and frozen until further processing for RNA isolation.

PMs were isolated by FACS from peritoneal lavage and cultured in RPMI complete medium supplemented with CSF2 (20 ng/ml) or CSF1 (20 ng/ml) (both STEMCELL Technologies) in non-tissue culture-treated 12-well plates. After 48 hours, the cells were lysed with RNA lysis buffer (Life Technologies), frozen on dry ice, and stored at  $-80^\circ\text{C}$  until further use.

AMs were isolated by BAL, seeded in RPMI complete medium in non-tissue culture-treated 12-well plates, and incubated at  $37^\circ\text{C}$  to allow AMs to adhere. After 4 hours, the medium was exchanged to remove nonadherent cells. AMs were cultured in RPMI complete medium without supplementation or supplemented with CSF2 (20 ng/ml; STEMCELL Technologies), CSF2 together with  $1 \mu\text{M}$  ruxolitinib (Tocris), or CSF1 (20 ng/ml; STEMCELL Technologies) according to the respective experimental setup. After 48 hours, cells were harvested for RNA isolation as described above.

### Luciferase reporter assay

Genomic regions of the *Pparg* locus were cloned from C57BL/6 DNA. The following primers were used to clone the following: the *Pparg1* promoter: 5'-TTCTCGAGCCCTCTCCACCC-TATGTGT-3' (forward) and 5'-GTAAGCTTGTCGTCA-CACTCGGT-3' (reverse); the *Pparg2* promoter: AGGACTCGAGCTTTTGTCTATTCT (forward) and 5'-CCAAAGCTTCACCCATAACAGCATAAA-3' (reverse); and the *Pparg* enhancer fragment: 5'-GTGAGCTCTAGGATTCTGTATT-CAGC-3' (forward) and 5'-TCCTCGAGGTGAGAATTTTGT-CAAGT-3' (reverse). The promoter fragments were cloned via Xho I/Hind III digest into the pGL4.10 (Promega) luciferase vector. The enhancer was cloned via Sac I/Xho I digest either alone or in front of the *Pparg2* promoter into pGL4.10. All clones were sequenced to verify cloning and sequences. For transfection,  $1 \times 10^4$  *Cebpb*-deficient MEF cells were plated into 96-well plates. The next day, 50 ng of test luciferase vector and different combinations of 50 ng of pcDNA3.1 (Addgene) containing either no gene (control) or LAP\*, LAP, or LIP were mixed and filled up to  $5 \mu\text{l}$  with serum-free medium. To control for transfection efficiency, we added 12.5 ng of *Renilla* luciferase (pGL4.70; Promega). Afterward,  $5 \mu\text{l}$  of serum-free medium containing  $1.1 \mu\text{l}$  of 7.5 mM polyethylenimine (PEI) (DNA:PEI ratio of 1:10) was added to the mix and incubated for 10 min. Ten microliters of transfection mix was carefully added to each well. Firefly luciferase and *Renilla* luciferase activity was measured with the Luc-Pair Duo-Luciferase HT Assay Kit (Genecopoeia) 48 hours after transfection according to the manufacturer's protocol. A Berthold luminometer (Centro LB 960) was used for measurement. All analysis was performed in duplicates, and all experiments were repeated twice with similar results.

### Quantification and statistical analysis

Statistical analysis (with the exception of RNA-seq, ATAC-seq, ChIPmentation, and lipidomic analyses; see respective sections in Materials and Methods for these analyses) was performed using the GraphPad Prism 6 software, and statistical tests were chosen according to assumptions considering data distribution and variance characteristics. To evaluate statistical differences between two groups, we applied a two-tailed *t* test with Welch's correction. For comparison of three groups, one-way analysis of variance (ANOVA) was used followed by multiple comparison correction with a Tukey test (in case of comparison of each group against every other group) or Dunnett's test (in case of comparison of all groups against a control group). Data in all experiments are depicted as means  $\pm$  SD, and statistical significance is presented as follows: not significant (n.s.),  $P > 0.05$ ; \* $P < 0.05$ ; \*\* $P < 0.01$ ; \*\*\* $P < 0.001$ . *n* indicates the number of animals used in the experiment, and each dot in the graphs corresponds to one animal.

### Supplementary Materials

This PDF file includes:

Figs. S1 to S7

Other Supplementary Material for this manuscript includes the following:

Data files S1 to S8

Data file S1

MDAR Reproducibility Checklist

[View/request a protocol for this paper from Bio-protocol.](#)

### REFERENCES AND NOTES

1. T. Hussels, T. J. Bell, Alveolar macrophages: Plasticity in a tissue-specific context. *Nat. Rev. Immunol.* **14**, 81–93 (2014).
2. B. C. Trapnell, J. A. Whitsett, K. Nakata, Pulmonary alveolar proteinosis. *N. Engl. J. Med.* **349**, 2527–2539 (2003).
3. D. Hashimoto, A. Chow, C. Noizat, P. Teo, M. B. Beasley, M. Leboeuf, C. D. Becker, P. See, J. Price, D. Lucas, M. Greter, A. Mortha, S. W. Boyer, E. C. Forsberg, M. Tanaka, N. van Rooijen, A. Garcia-Sastre, E. R. Stanley, F. Ginhoux, P. S. Frenette, M. Merad, Tissue-resident macrophages self-maintain locally throughout adult life with minimal contribution from circulating monocytes. *Immunity* **38**, 792–804 (2013).
4. M. Guillems, I. De Kleer, S. Henri, S. Post, L. Vanhoutte, S. De Prijck, K. Deswarte, B. Malissen, H. Hammad, B. N. Lambrecht, Alveolar macrophages develop from fetal monocytes that differentiate into long-lived cells in the first week of life via GM-CSF. *J. Exp. Med.* **210**, 1977–1992 (2013).
5. M. Cohen, A. Giladi, A.-D. Gorki, D. G. Solodkin, M. Zada, A. Hladik, A. Miklosi, T.-M. Salame, K. B. Halpern, E. David, S. Itzkovitz, T. Harkany, S. Knapp, I. Amit, Lung single-cell signaling interaction map reveals basophil role in macrophage imprinting. *Cell* **175**, 1031–1044.e18 (2018).
6. V. Goss, A. N. Hunt, A. D. Postle, Regulation of lung surfactant phospholipid synthesis and metabolism. *Biochim. Biophys. Acta* **1831**, 448–458 (2013).
7. C. Schneider, S. P. Nobs, M. Kurrer, H. Rehrauer, C. Thiele, M. Kopf, Induction of the nuclear receptor PPAR- $\gamma$  by the cytokine GM-CSF is critical for the differentiation of fetal monocytes into alveolar macrophages. *Nat. Immunol.* **15**, 1026–1037 (2014).
8. M. Straccia, N. Gresa-Arribas, G. Dentesano, A. Ejarque-Ortiz, J. M. Tusell, J. Serratos, C. Solà, J. Saura, Pro-inflammatory gene expression and neurotoxic effects of activated microglia are attenuated by absence of CCAAT/enhancer binding protein  $\beta$ . *J. Neuroinflammation* **8**, 156 (2011).
9. A. Ndoja, R. Reja, S.-H. Lee, J. D. Webster, H. Ngu, C. M. Rose, D. S. Kirkpatrick, Z. Modrusan, Y.-J. J. Chen, D. L. Dugger, V. Gandham, L. Xie, K. Newton, V. M. Dixit, Ubiquitin ligase COP1 suppresses neuroinflammation by degrading c/EBP $\beta$  in microglia. *Cell* **182**, 1156–1169.e12 (2020).

10. H. Hirai, P. Zhang, T. Dayaram, C. J. Hetherington, S.-I. Mizuno, J. Imanishi, K. Akashi, D. G. Tenen, C/EBPbeta is required for "emergency" granulopoiesis. *Nat. Immunol.* **7**, 732–739 (2006).
11. A. Mildner, J. Schönheit, A. Giladi, E. David, D. Lara-Astiaso, E. Lorenzo-Vivas, F. Paul, L. Chappell-Maor, J. Priller, A. Leutz, I. Amit, S. Jung, Genomic characterization of murine monocytes reveals C/EBPβ transcription factor dependence of Ly6C<sup>−</sup> cells. *Immunity* **46**, 849–862.e7 (2017).
12. D. W. Cain, E. G. O'Koren, M. J. Kan, M. Womble, G. D. Sempowski, K. Hopper, M. D. Gunn, G. Kelseo, Identification of a tissue-specific, C/EBPβ-dependent pathway of differentiation for murine peritoneal macrophages. *J. Immunol.* **191**, 4665–4675 (2013).
13. E. L. Gautier, T. Shay, J. Miller, M. Greter, C. Jakubzick, S. Ivanov, J. Helft, A. Chow, K. G. Elpek, S. Gordonov, A. R. Mazloom, A. Ma'ayan, W.-J. Chua, T. H. Hansen, S. J. Turley, M. Merad, G. J. Randolph; Immunological Genome Consortium, Gene-expression profiles and transcriptional regulatory pathways that underlie the identity and diversity of mouse tissue macrophages. *Nat. Immunol.* **13**, 1118–1128 (2012).
14. Z. Liu, Y. Gu, S. Chakarov, C. Blieriot, I. Kwok, X. Chen, A. Shin, W. Huang, R. J. Dress, C.-A. Dutertre, A. Schlitzer, J. Chen, L. G. Ng, H. Wang, Z. Liu, B. Su, F. Ginhoux, Fate mapping via Ms4a3-expression history traces monocyte-derived cells. *Cell* **178**, 1509–1525.e19 (2019).
15. Z. Liu, Y. Gu, S. Chakarov, C. Blieriot, X. Chen, A. Shin, W. Huang, Fate mapping via Ms4a3 expression history traces monocyte-derived cells. *bioRxiv* (2019). 652032.
16. R. Kühn, F. Schwenk, M. Aguet, K. Rajewsky, Inducible gene targeting in mice. *Science* **269**, 1427–1429 (1995).
17. C. L. Abram, G. L. Roberge, Y. Hu, C. A. Lowell, Comparative analysis of the efficiency and specificity of myeloid-Cre deleting strains using ROSA-EYFP reporter mice. *J. Immunol. Methods* **408**, 89–100 (2014).
18. L. van de Laar, W. Saelens, S. De Prijck, L. Martens, C. L. Scott, G. Van Isterdael, E. Hoffmann, R. Beyaert, Y. Saeys, B. N. Lambrecht, M. Guillemins, Yolk sac macrophages, fetal liver, and adult monocytes can colonize an empty niche and develop into functional tissue-resident macrophages. *Immunity* **44**, 755–768 (2016).
19. K. Wethmar, J. J. Smink, A. Leutz, Upstream open reading frames: Molecular switches in (patho)physiology. *Bioessays* **32**, 885–893 (2010).
20. V. Bégay, J. J. Smink, C. Loddenkemper, K. Zimmermann, C. Rudolph, M. Scheller, D. Steinemann, U. Leser, B. Schlegelberger, H. Stein, A. Leutz, Deregulation of the endogenous C/EBPβ LIP isoform predisposes to tumorigenesis. *J. Mol. Med. (Berl)* **93**, 39–49 (2015).
21. C. Schmidl, A. F. Rendeiro, N. C. Sheffield, C. Bock, ChIPmentation: Fast, robust, low-input ChIP-seq for histones and transcription factors. *Nat. Methods* **12**, 963–965 (2015).
22. J. D. Buenostro, P. G. Giresi, L. C. Zaba, H. Y. Chang, W. J. Greenleaf, Transposition of native chromatin for fast and sensitive epigenomic profiling of open chromatin, DNA-binding proteins and nucleosome position. *Nat. Methods* **10**, 1213–1218 (2013).
23. A. Shemer, J. Grozovski, T. L. Tay, J. Tao, A. Volaski, P. Süß, A. Arduara-Fabregat, M. Gross-Vered, J.-S. Kim, E. David, L. Chappell-Maor, L. Thielecke, C. K. Glass, K. Cornils, M. Prinz, S. Jung, Engrafted parenchymal brain macrophages differ from microglia in transcriptome, chromatin landscape and response to challenge. *Nat. Commun.* **9**, 5206 (2018).
24. A. Vidal-Puig, M. Jimenez-Liñan, B. B. Lowell, A. Hamann, E. Hu, B. Spiegelman, J. S. Flier, D. E. Moller, Regulation of PPAR gamma gene expression by nutrition and obesity in rodents. *J. Clin. Invest.* **97**, 2553–2561 (1996).
25. E. M. Todd, J. Y. Zhou, T. P. Szasz, L. E. Deady, J. A. D'Angelo, M. D. Cheung, A. H. J. Kim, S. C. Morley, Alveolar macrophage development in mice requires L-plastin for cellular localization in alveoli. *Blood* **128**, 2785–2796 (2016).
26. M. I. Lefterova, Y. Zhang, D. J. Steger, M. Schupp, J. Schug, A. Cristancho, D. Feng, D. Zhuo, C. J. Stoeckert, X. S. Liu, M. A. Lazar, PPARγ and C/EBP factors orchestrate adipocyte biology via adjacent binding on a genome-wide scale. *Genes Dev.* **22**, 2941–2952 (2008).
27. S. Watanabe, T. Itoh, K. Arai, Roles of JAK kinases in human GM-CSF receptor signal transduction. *J. Allergy Clin. Immunol.* **98**, S183–S191 (1996).
28. A. Mortha, A. Chudnovskiy, D. Hashimoto, M. Bogunovic, S. P. Spencer, Y. Belkaid, M. Merad, Microbiota-dependent crosstalk between macrophages and ILC3 promotes intestinal homeostasis. *Science* **343**, 1249288–1249288 (2014).
29. L. Robb, C. C. Drinkwater, D. Metcalf, R. Li, F. Köntgen, N. A. Nicola, C. G. Begley, Hematopoietic and lung abnormalities in mice with a null mutation of the common beta subunit of the receptors for granulocyte-macrophage colony-stimulating factor and interleukins 3 and 5. *Proc. Natl. Acad. Sci. U.S.A.* **92**, 9565–9569 (1995).
30. B. Becher, A. Schlitzer, J. Chen, F. Mair, H. R. Sumatoto, K. W. W. Teng, D. Low, C. Ruedl, P. Riccardi-Castagnoli, M. Poidinger, M. Greter, F. Ginhoux, E. W. Newell, High-dimensional analysis of the murine myeloid cell system. *Nat. Immunol.* **15**, 1181–1189 (2014).
31. X. Ma, D. Wang, W. Zhao, L. Xu, Deciphering the roles of PPARγ in adipocytes via dynamic change of transcription complex. *Front. Endocrinol.* **9**, 473 (2018).
32. J. E. Merrett, T. Bo, P. J. Psaltis, C. G. Proud, Identification of DNA response elements regulating expression of CCAAT/enhancer-binding protein (C/EBP) β and δ and MAP kinase-interacting kinases during early adipogenesis. *Adipocyte* **9**, 427–442 (2020).
33. D. J. Steger, G. R. Grant, M. Schupp, T. Tomaru, M. I. Lefterova, J. Schug, E. Manduchi, C. J. Stoeckert, M. A. Lazar, Propagation of adipogenic signals through an epigenomic transition state. *Genes Dev.* **24**, 1035–1044 (2010).
34. T. Tanaka, N. Yoshida, T. Kishimoto, S. Akira, Defective adipocyte differentiation in mice lacking the C/EBPbeta and/or C/EBPdelta gene. *EMBO J.* **16**, 7432–7443 (1997).
35. D. Ren, T. N. Collingwood, E. J. Rebar, A. P. Wolffe, H. S. Camp, PPARgamma knockdown by engineered transcription factors: Exogenous PPARgamma2 but not PPARgamma1 reactivates adipogenesis. *Genes Dev.* **16**, 27–32 (2002).
36. Q.-Q. Tang, M. Grønberg, H. Huang, J.-W. Kim, T. C. Otto, A. Pandey, M. D. Lane, Sequential phosphorylation of CCAAT enhancer-binding protein beta by MAPK and glycogen synthase kinase 3beta is required for adipogenesis. *Proc. Natl. Acad. Sci. U.S.A.* **102**, 9766–9771 (2005).
37. C. Nieto, R. Bragado, C. Municio, E. Sierra-Filardi, B. Alonso, M. M. Escribese, J. Domínguez-Andrés, C. Ardavin, A. Castrillo, M. A. Vega, A. Puig-Kröger, A. L. Corbí, The activin A-peroxisome proliferator-activated receptor gamma axis contributes to the transcriptome of GM-CSF-conditioned human macrophages. *Front. Immunol.* **9**, 31 (2018).
38. Y. Lavin, D. Winter, R. Blecher-Gonen, E. David, H. Keren-Shaul, M. Merad, S. Jung, I. Amit, Tissue-resident macrophage enhancer landscapes are shaped by the local microenvironment. *Cell* **159**, 1312–1326 (2014).
39. C. Bornstein, D. Winter, Z. Barnett-Itzhaki, E. David, S. Kadri, M. Garber, I. Amit, A negative feedback loop of transcription factors specifies alternative dendritic cell chromatin states. *Mol. Cell* **56**, 749–762 (2014).
40. R. Siersbæk, R. Nielsen, S. John, M.-H. Sung, S. Baek, A. Loft, G. L. Hager, S. Mandrup, Extensive chromatin remodelling and establishment of transcription factor "hotspots" during early adipogenesis. *EMBO J.* **30**, 1459–1472 (2011).
41. V. Bégay, C. Baumeier, K. Zimmermann, A. Heuser, A. Leutz, The C/EBPβ LIP isoform rescues loss of C/EBPβ function in the mouse. *Sci. Rep.* **8**, 8417 (2018).
42. C.-H. Lee, R. M. Evans, Peroxisome proliferator-activated receptor-γ in macrophage lipid homeostasis. *Trends Endocrinol. Metab.* **13**, 331–335 (2002).
43. E. L. Gautier, A. Chow, R. Spanbroek, G. Marcelin, M. Greter, C. Jakubzick, M. Bogunovic, M. Leboeuf, N. van Rooijen, A. J. Habenicht, M. Merad, G. J. Randolph, Systemic analysis of PPARγ in mouse macrophage populations reveals marked diversity in expression with critical roles in resolution of inflammation and airway immunity. *J. Immunol.* **189**, 2614–2624 (2012).
44. J. C. Cronk, A. J. Filiano, A. Louveau, I. Marin, R. Marsh, E. Ji, D. H. Goldman, I. Smirnov, N. Geraci, S. Acton, C. C. Overall, J. Kipnis, Peripherally derived macrophages can engraft the brain independent of irradiation and maintain an identity distinct from microglia. *J. Exp. Med.* **215**, 1627–1647 (2018).
45. E. Sterneck, L. Tassarollo, P. F. Johnson, An essential role for C/EBPbeta in female reproduction. *Genes Dev.* **11**, 2153–2162 (1997).
46. B. E. Clausen, C. Burkhardt, W. Reith, R. Renkawitz, I. Förster, Conditional gene targeting in macrophages and granulocytes using LysMcre mice. *Transgenic Res.* **8**, 265–277 (1999).
47. P. B. Stranges, J. Watson, C. J. Cooper, C.-M. Choisy-Rossi, A. C. Stonebraker, R. A. Beighton, H. Hartig, J. P. Sundberg, S. Servick, G. Kaufmann, P. J. Fink, A. V. Chervonsky, Elimination of antigen-presenting cells and autoreactive T cells by Fas contributes to prevention of autoimmunity. *Immunity* **26**, 629–641 (2007).
48. E. Sterneck, S. Zhu, A. Ramirez, J. L. Jorcano, R. C. Smart, Conditional ablation of C/EBP beta demonstrates its keratinocyte-specific requirement for cell survival and mouse skin tumorigenesis. *Oncogene* **25**, 1272–1276 (2006).
49. D. A. Jaitin, E. Kenigsberg, H. Keren-Shaul, N. Elefant, F. Paul, I. Zaretsky, A. Mildner, N. Cohen, S. Jung, A. Tanay, I. Amit, Massively parallel single-cell RNA-Seq for marker-free decomposition of tissues into cell types. *Science* **343**, 776–779 (2014).
50. E. M. Lyras, K. Zimmermann, L. K. Wagner, D. Dörr, C. S. N. Klose, C. Fischer, S. Jung, S. Yona, A.-H. Hovav, W. Stenzel, S. Dommerich, T. Conrad, A. Leutz, A. Mildner, Tongue immune compartment analysis reveals spatial macrophage heterogeneity. *Elife* **11**, 265–277 (2022).
51. D. Lara-Astiaso, A. Weiner, E. Lorenzo-Vivas, I. Zaretsky, D. A. Jaitin, E. David, H. Keren-Shaul, A. Mildner, D. Winter, S. Jung, N. Friedman, I. Amit, Immunogenetics. Chromatin state dynamics during blood formation. *Science* **345**, 943–949 (2014).
52. H. Li, Aligning sequence reads, clone sequences and assembly contigs with BWA-MEM. *arXiv:1303.3997v2 [q-bio.GN]* (26 May 2013).
53. R. Stark, G. Brown, DiffBind: Differential binding analysis of ChIP-Seq peak data; bioconductor.statistik.tu-dortmund.de.
54. J. M. Gaspar, Improved peak-calling with MACS2. *bioRxiv* , 496521 (2018).
55. M. I. Love, W. Huber, S. Anders, Moderated estimation of fold change and dispersion for RNA-seq data with DESeq2. *Genome Biol.* **15**, 550 (2014).

56. G. Yu, L.-G. Wang, Q.-Y. He, ChIPseeker: An R/Bioconductor package for ChIP peak annotation, comparison and visualization. *Bioinformatics* **31**, 2382–2383 (2015).
57. O. Fornes, J. A. Castro-Mondragon, A. Khan, R. van der Lee, X. Zhang, P. A. Richmond, B. P. Modi, S. Correard, M. Gheorghe, D. Baranašić, W. Santana-Garcia, G. Tan, J. Chèneby, B. Ballester, F. Parcy, A. Sandelin, B. Lenhard, W. W. Wasserman, A. Mathelier, JASPAR 2020: Update of the open-access database of transcription factor binding profiles. *Nucleic Acids Res.* **48**, D87–D92 (2020).
58. T. Domaszewska, L. Scheuermann, K. Hahnke, H. Mollenkopf, A. Dorhoi, S. H. E. Kaufmann, J. Weiner III, Concordant and discordant gene expression patterns in mouse strains identify best-fit animal model for human tuberculosis. *Sci. Rep.* **7**, 12094–12013 (2017).
59. H. Xu, X. Luo, J. Qian, X. Pang, J. Song, G. Qian, J. Chen, S. Chen, D. Doucet, FastUniq: A fast de novo duplicates removal tool for paired short reads. *PLOS ONE* **7**, e52249 (2012).
60. A. Dobin, C. A. Davis, F. Schlesinger, J. Drenkow, C. Zaleski, S. Jha, P. Batut, M. Chaisson, T. R. Gingeras, STAR: Ultrafast universal RNA-seq aligner. *Bioinformatics* **29**, 15–21 (2013).
61. Y. Liao, G. K. Smyth, W. Shi, featureCounts: An efficient general purpose program for assigning sequence reads to genomic features. *Bioinformatics* **30**, 923–930 (2014).
62. M. Stephens, False discovery rates: A new deal. *Biostatistics* **18**, 275–294 (2017).
63. Z. Gu, R. Eils, M. Schlesner, Complex heatmaps reveal patterns and correlations in multi-dimensional genomic data. *Bioinformatics* **32**, 2847–2849 (2016).
64. G. Yu, L.-G. Wang, Y. Han, Q.-Y. He, clusterProfiler: An R package for comparing biological themes among gene clusters. *OMICS* **16**, 284–287 (2012).
65. J. T. Leek, W. E. Johnson, H. S. Parker, A. E. Jaffe, J. D. Storey, The sva package for removing batch effects and other unwanted variation in high-throughput experiments. *Bioinformatics* **28**, 882–883 (2012).
66. M. E. Ritchie, B. Hipson, D. Wu, Y. Hu, C. W. Law, W. Shi, G. K. Smyth, limma powers differential expression analyses for RNA-sequencing and microarray studies. *Nucleic Acids Res* **43**, e47 (2015).

**Acknowledgments:** We thank V. Malchin, S. Jaksch, and J. Voß for excellent technical support, as well as the MDC animal facility, especially J. Bergemann, the MDC FACS core unit, H.-P. Rahn, and the MDC genomic core facility, especially D. Sunaga-Franze. We thank E. Kowenz-Leutz for the donation of C/EBPβ expression constructs and I. Amit for support. The *Csf2rb*<sup>-/-</sup> line was kindly provided by M. Sieweke (Center for Regenerative Therapies, Dresden, Germany). We also thank C. J. L. Elender and J. Favret for technical advice and S. Yona and S. Jung for discussion. Computation has been performed on the HPC for Research Cluster of the Berlin Institute of Health. **Funding:** D.D. was funded by the international MDC PhD program and received a travel grant from Boehringer Ingelheim Fonds. A.M. was a Heisenberg fellow supported by the DFG (MI1328/3-1). A.M. was financially supported by the InFLAMES Flagship Programme of the Academy of Finland (decision number: 337530). **Author contributions:** D.D. performed most experiments and analysis. B.O. and J.M.W. were supervised by D.B. and performed bioinformatic analyses. A.M., L.K.W., E.M.L., V.S., and K.Z. helped with experiments and analysis. C.A. and D.G.L. performed ChIPmentation experiments. R.L., D.L.-A., F.P., and U.E.H. provided mouse lines and technical expertise. A.L. provided financial support, laboratory space, supervision, discussion, review, and editing. A.M. designed and supervised the study. D.D. and A.M. wrote the manuscript. **Competing interests:** The authors declare that they have no competing interests. **Data and materials availability:** All data needed to evaluate the conclusions in the paper are present in the paper or the Supplementary Materials. Sequencing data that were generated within this study have been deposited in the GEO database with the accession code GSE173970. Microarray data of CD11c-Cre *Pparg* flox and control AMs used for transcriptomic comparison to *Cebpb* KO AMs were downloaded from GEO (GSE60249).

Submitted 14 April 2021

Resubmitted 22 March 2022

Accepted 22 August 2022

Published 16 September 2022

10.1126/sciimmunol.abj0140

## **C/EBP# regulates lipid metabolism and *Pparg* isoform 2 expression in alveolar macrophages**

Dorothea Drr, Benedikt Obermayer, January Mikolaj Weiner, Karin Zimmermann, Chiara Anania, Lisa Katharina Wagner, Ekaterini Maria Lyras, Valeriia Sapozhnikova, David Lara-Astiaso, Felipe Prsper, Roland Lang, Daro G. Lupiez, Dieter Beule, Uta E. Hpken, Achim Leutz, and Alexander Mildner

*Sci. Immunol.*, **7** (75), eabj0140.  
DOI: 10.1126/sciimmunol.abj0140

### **Alveolar macrophage development and function**

Alveolar macrophages (AMs) are specialized macrophages that serve several key functions in the lung. Here, Dörr *et al.* used transcriptomic, ChIPmentation, and chromatin accessibility analysis to demonstrate that the transcription factor CCAAT/enhancer binding protein beta (C/EBP#) is required for AM development. C/EBP#-deficient AMs had defects in proliferation, lipid metabolism, and phagocytosis, thus causing mice to have symptoms that resemble pulmonary alveolar proteinosis (PAP). They observed that the long C/EBP# protein variants LAP\* and LAP, combined with CSF2 signaling, induced specific expression of *Pparg* isoform 2, which is a mechanism that they also observed in other CSF2-primed macrophages. These findings indicate that C/EBP# is a key regulator of AM development and lipid metabolism.

### **View the article online**

<https://www.science.org/doi/10.1126/sciimmunol.abj0140>

### **Permissions**

<https://www.science.org/help/reprints-and-permissions>

Use of this article is subject to the [Terms of service](#)

---

*Science Immunology* (ISSN ) is published by the American Association for the Advancement of Science. 1200 New York Avenue NW, Washington, DC 20005. The title *Science Immunology* is a registered trademark of AAAS.

Copyright © 2022 The Authors, some rights reserved; exclusive licensee American Association for the Advancement of Science. No claim to original U.S. Government Works